INFORMATION TO USERS

This manuscript has been reproduced from the microfilm master. UMI films the text directly from the original or copy submitted. Thus, some thesis and dissertation copies are in typewriter face, while others may be from any type of computer printer.

The quality of this reproduction is dependent upon the quality of the copy submitted. Broken or indistinct print, colored or poor quality illustrations and photographs, print bleedthrough, substandard margins, and improper alignment can adversely affect reproduction.

In the unlikely event that the author did not send UMI a complete manuscript and there are missing pages, these will be noted. Also, if unauthorized copyright material had to be removed, a note will indicate the deletion.

Oversize materials (e.g., maps, drawings, charts) are reproduced by sectioning the original, beginning at the upper left-hand corner and continuing from left to right in equal sections with small overlaps. Each original is also photographed in one exposure and is included in reduced form at the back of the book.

Photographs included in the original manuscript have been reproduced xerographically in this copy. Higher quality 6" x 9" black and white photographic prints are available for any photographs or illustrations appearing in this copy for an additional charge. Contact UMI directly to order.

UMI®

Bell & Howell Information and Learning
300 North Zeeb Road, Ann Arbor, MI 48106-1346 USA
800-521-0600

II-VI Compound Semiconductor Lasers and Light Emitting Diodes

by

Yongming Guo

A dissertation submitted to the Graduate Faculty in Physics in partial fulfillment of the requirements for the degree of Doctor of Philosophy, The City University of New York

1999

This manuscript has been read and accepted for the Graduate Faculty in Physics in satisfaction of the dissertation requirement for the degree of Doctor of Philosophy.

6/14/99 Ying-Chih Chen
Date Professor Ying-Chih Chen, Chair of Examining Committee

6/15/99 Louis Celenza
Date Professor Louis Celenza, Executive Officer

Professor Janos Bergou

Professor Godfrey Gumbs

Professor Mark Hillery

Professor Maria Tamargo

Supervisory Committee

THE CITY UNIVERSITY OF NEW YORK

Abstract

II-VI compound semiconductor lasers and light emitting diodes

by

Yongming Guo

Advisor: Professor Ying-Chih Chen

The II-VI compound semiconductors based on ZnCdSe/ZnCdMgSe quantum wells grown on InP are promising materials for fabricating light-emitting devices operating in the visible spectral region. A unique feature of these materials is that the epitaxial layers can be grown lattice-matched to InP, resulting superior material quality. By tailoring the thickness and composition of the quantum well, the emission wavelength covers most of the visible spectrum. In this thesis, the optical and electronic properties of the ZnCdSe/ZnCdMgSe quantum-well materials and devices are reported. Various device design issues, such as carrier confinement, modal confinement, and electrical contact, are discussed. Using photo-pumping, laser action in red, green, and blue has been demonstrated. The newly developed p-contact technology also resulted in the operation of the first p-n junction light-emitting diode. The observed emission wavelength and waveguiding properties of the devices are consistent with those projected according to the design parameters.

To
my wife Yan Fan
and our daughter Liangjie Guo

Acknowledgements

I would like to thank my advisor, Professor Ying-Chih Chen, for his invaluable guidance and support. During the past few years, I have learned a great deal of experimental skills and problem solving techniques, which is never taught in books, from him. His encouragement and inspiration guide me through many obstacles in the research of this thesis. I really appreciate being working in his optics lab.

I would also like to express my deeply gratitude to Professor Maria Tamargo and her group at the City College, especially Mr. Linfei Zeng and Mr. Weichen Lin for providing the laser materials and light emitting diodes and contributing the low-temperature photoluminescence measurement and I-V measurement of the LEDs.

Many thanks to Professor Godfrey Gumbs for his encouragement and many informative discussions concerning my research work. His contribution in the calculation of second-order non-linear optical susceptibility is greatly appreciated. Unfortunately much of the work done in that area is not included in this thesis due to the consideration of focusing the contents of the thesis to the specific topic on lasers and light emitting diodes.

Thanks to all the faculty and staff members in the Physics Department of Hunter College for providing a wonderful and enjoyable environment for research and study.

Table of Contents

List of Tables

List of Figures

Chapter 1 Introduction

Recently, the development of semiconductor laser diodes emitting in the visible spectral region has attracted considerable interest due to the wide application of visible lasers in display, printing and optical recording. Two direct bandgap semiconductor systems, based on II-VI compounds, such as ZnSe, and III-V compounds, such as GaN, are well suited for generating visible radiation. In this thesis we will concentrate on the development of light-emitting devices based on II-VI compound semiconductors.

The early experiments on ZnSe-based materials have confronted many difficult problems, some of which are intrinsic to the wide-bandgap materials in general, such as doping. With a larger bandgap, the possibility exists of creating and then ionizing vacancies, causing self-compensation of the material. Other problems are material-specific, such as finding a heterostructure suitable for fabricating the active region of a short-wavelength laser and suitable waveguide materials for optical confinement. As a result, by the late 1970's the work on the II-VI semiconductors was largely relegated to a small community of researchers. In the early 80's, research efforts were primarily focused on non-equilibrium epitaxial growth methods, such as molecular-beam epitaxy (MBE) growth of II-VI heterostructure semiconductors.

The success [1][2] in achieving stable p-type doping in ZnSe and the progress[3]-[7] in MBE growth technique of II-VI multilayer by the end of the 1980's renewed wide interest in using the II-VI compound semiconductor for laser applications.

In 1991, a research group of 3M company reported the first ZnCdSe/ZnSe-based visible semiconductor laser operation at 77 K. [8] The following list summarizes the major breakthroughs in the development of ZnSe-based wide bandgap laser diodes[9]-[13] since 1991.

1991 The first blue-green laser diodes based on ZnCdSe/ZnSe operating at 77 K was demonstrated. The lifetime was several seconds.

1992 The improvement in electrical contacts and optical and electrical confinement resulted in the first blue emitting laser diodes operating at 77 K.

1993 Blue-green laser diodes using ZnMgSSe as the cladding layer and pseudomorphic quantum-well structure operating at room temperature were demonstrated.

1994 Continuous wave operation (CW) at room temperature of blue-green laser diodes was reported. The lifetimes reached several minutes in

the CW operation and several hours in pulsed operation.

1996 Greatly improved lifetime of 100 hours (blue-green) in the CW operation at room temperature was reported. The defect density of the material was reduced to 3×10^3 cm^{-3}

1997 Improved electrical contact resulted in a device lifetime of 400 hours.

To date, most of the reported blue-green lasers are made of $Zn_{1-x}Cd_xSe$/ $Zn_{1-x}Mg_xS_ySe_{1-y}$ grown on GaAs substrates. In this material system, although the cladding and waveguiding layers can be grown lattice matched to the substrate, a large lattice mismatch exists between the ZnCdSe quantum-well layer and GaAs. The large lattice mismatch produces strain, which affects the quality of the material and may result in early degradation of the laser device. One of the possible causes of rapid degradation of the device is the dark-line defect forming in the active layer from pre-existing defects of the material [14][15]. The presence of the strain in the active region may promote defect propagation and dark line formation.

On the other hand, recent progress [16]-[18] in the growth of ternary ZnCdSe and ZnSeTe and quaternary ZnCdMgSe materials on InP substrates points to an alternative for the visible lasers. The use of InP as the substrate material

makes it possible to select among a set of new II-VI quaternary and ternary materials for the quantum-well and barrier layers that can be all lattice-matched to the substrate. This offers great promise in terms of improved crystalline quality and reliability over the II-VI materials that have previously been used to fabricate blue-green lasers. The absence of strain also allows the fabrication of multiple quantum-well lasers from these materials without being limited by the critical thickness. In addition, the room temperature bandgap for the ZnCdMgSe quaternary system ranges from 2.1 eV to over 3 eV. Thus, by controlling the thickness of the quantum-well and/or the composition of the material in lattice-matched ZnCdSe/ZnCdMgSe quantum-well structures, the emission wavelength can be made to vary over a wide spectral range from red to blue.[19] This feature allows lasers that emit over most of the visible range to be fabricated from these materials.

Using the photo-pumping technique, we have achieved laser action in ZnCdMgSe quantum-well lasers emitting in red, green and blue. This result points to the possibility of fabricating fully-integrated white light sources and full color display arrays containing red, green and blue in each pixel for a variety of applications. Currently, no other single semiconductor material system has been shown to provide full-color visible emission. More

recently, light-emitting diodes with electro-luminescence emitting in red, blue and green have also been developed.

In this thesis, a brief review of the development of the II-VI semiconductor laser diodes and light-emitting diodes is given in Chapter 2. The results of the photoluminescence and photo-pumping lasing experiments are described in Chapter 3. The results of the electro-luminescence spectra and current-voltage characteristic of ZnCdSe/ZnCdMgSe light-emitting diodes are discussed in Chapter 4. The gain profiles of ZnCdSe/ZnCdMgSe quantum-well lasers are illustrated in chapter 5. A summary of my research and the technological outlook is presented in Chapter 6.

Chapter 2 Background

2.1 Basics of semiconductor lasers

2.1.1 Structure of semiconductor lasers

There are two necessary conditions to operate a semiconductor laser device: (1) a gain medium that can amplify the electromagnetic radiation, and (2) a waveguiding mechanism that can confine the electromagnetic field in a well-defined waveguide mode. In a semiconductor laser, the gain medium is a thin layer of semiconductor, which can emit and amplify the electromagnetic radiation. The waveguide is formed by the built-in structure of the refractive index profile. The two cleaved facets of the semiconductor wafer form the laser resonator. The typical structure of a semiconductor laser is shown in Figure 2.1.

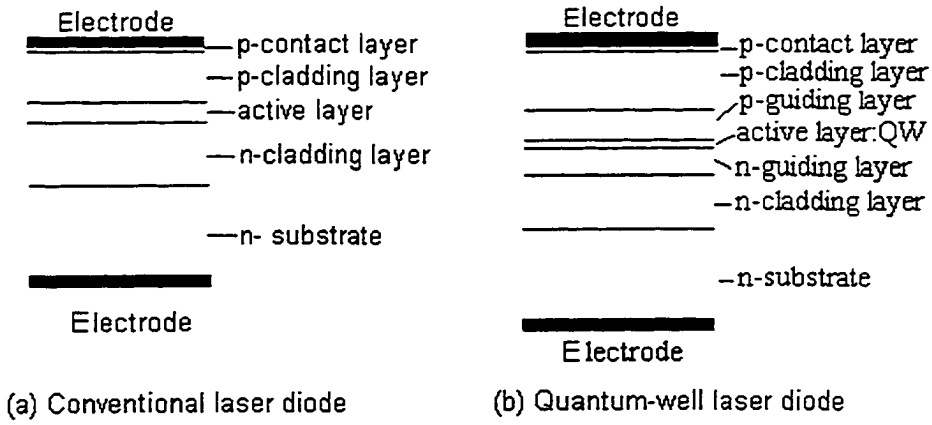

Figure 2.1. Schematic structure of (a) conventional semiconductor laser diode and (b) quantum-well laser diode.

The laser consists of a thin active layer, which is sandwiched between two cladding layers with higher bandgap energy. In a conventional semiconductor laser diode, the thickness of the active layer is typically in the range of 0.1-0.3 μm. The functions of the higher energy bandgap for the cladding layer are to provide the energy barrier needed for carrier confinement and to provide waveguiding for optical confinement for the electromagnetic radiation.

In general, the band alignment at the hetero-junction can be type-I or type-II, as illustrated in Figure 2.2. In order to provide effective carrier confinement in the active layer, the band alignment must be of the type-I, as shown in Figure 2.3.

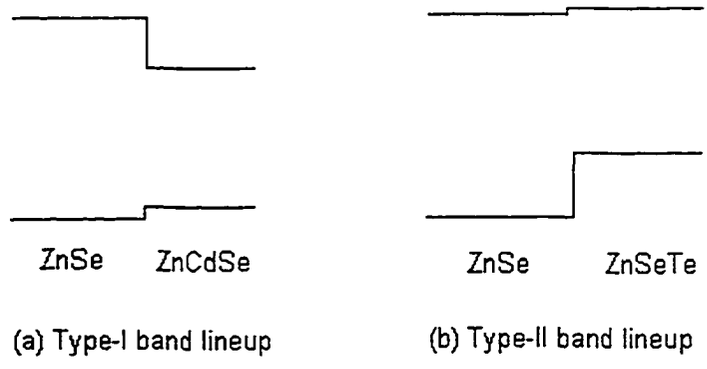

Figure 2.2 Band lineup of (a) type-I hetero-junction and (b) type-II hetero-junction.

When the thickness of the active layer is comparable to the de Broglie wavelength of the carriers, the kinetic energy of the carriers associated with the motion in the direction perpendicular to the layer is quantized, giving rise to a set of discrete energy levels. The quantum effect becomes pronounced when the well thickness is less than 10 nm. The major benefit resulting from the use of the quantum well structure is the increased density of states near the bandgap, which helps reduce the number of carriers needed to achieve optical transparency in the active layer. Thus the threshold current for laser operation is reduced by approximately the ratio of the thicknesses of the active layers.

In quantum-well laser diodes, the thin quantum well cannot provide effective waveguiding because the thickness of the quantum well is much smaller than the wavelength of light. It is often necessary to insert a waveguiding layer between the cladding layer and active layer to increase the overlap between the electromagnetic radiation and the quantum well.

Figure 2.3 shows the schematic of bandgap energy and refractive-index profiles of a quantum-well laser. Figure 2.3 (a) is the desired band lineup for the cladding, waveguiding and quantum well layers. The quantum well

has the smallest bandgap energy while cladding layers have the largest bandgap energy to confine electrons and holes. Figure 2.3 (b) is the

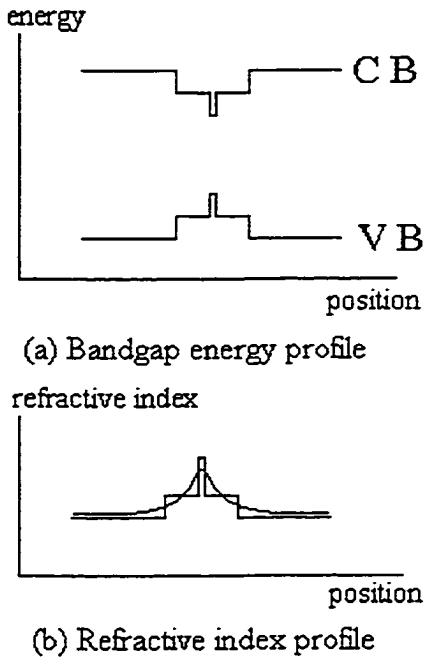

Figure 2.3. (a) Bandgap energy and (b) refractive-index profiles of a quantum-well structure. The curve shown in (b) is the calculated modal profile of the fundamental transverse mode of the waveguide.

corresponding refractive-index profile. The quantum well has the largest index of refraction and the cladding layers have the smallest index of refraction. The effectiveness of optical confinement in such a waveguide depends on the difference of the refractive indices between adjacent layers and the thickness of each layer. The details of the optical confinement techniques will be discussed in Chapter 2.1.4

2.1.2 p-n heterojunction

The schematic band profiles for ZnCdSe/ZnSSe/ZnMgSSe heterostructures are shown in Figure 2.4. An undoped quantum-well structure is shown in (a). The band offset between the quantum well and the waveguide layers, ΔE_c and ΔE_v, forms the potential barriers which confine the carriers in the well. The dashed line in the middle is the Fermi level. Figure 2.4 (b) shows the band profile with heavily doped cladding layers and lightly doped waveguiding layers. The energy band in the vicinity of the p-n junction is tilted due to the built-in potential difference between the p-side and n-side. Under forward bias in (c), the potential barriers are reduced so that electrons and holes are driven into the quantum well layer where they recombine to emit photons.

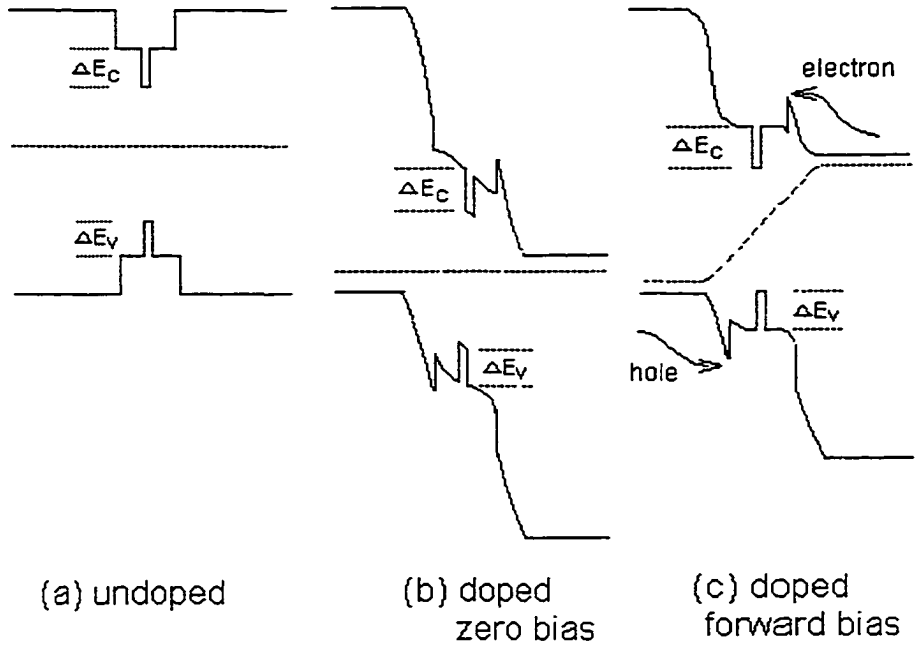

Figure 2.4 Schematic band profiles for ZnCdSe/ZnSSe/ZnMgSSe heterostructures with (a) undoped layers, (b) doped layers to form a p-n junction, and (c) p-n junction under forward bias.

2.1.3. The condition for laser threshold[20]

Consider the interband transition shown in Figure 2.5 for a direct bandgap semiconductor material in the presence of an incident photon whose energy is:

$$E = h\nu = E_c + E_v + E_g \tag{2.1}$$

Where E_g is the bandgap, E_c is the energy of the electron in the conduction band, E_v is the energy of the hole in the valence band, and $h\nu$ is the photon energy.

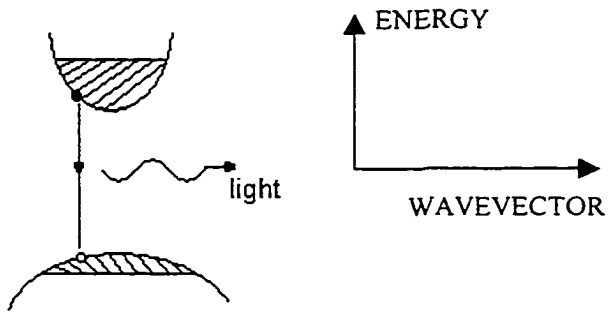

Figure 2.5 Interband transition in a direct bandgap semiconductor material.

The occupation probability of an electron with energy E_c follows the Fermi-Dirac distribution function given by

$$f_c(E_c) = \frac{1}{e^{(E_c - E_{Fc})/kT} + 1} \tag{2.2}$$

where E_{Fc} is the quasi-Fermi energy for the conduction band, k is Boltzmann constant, and T is the absolute temperature. Similarly, for the

holes in the valence band, the occupation probability of a hole with energy E_v is given by

$$f_v(E_v) = \frac{1}{e^{(E_v - E_{Fv})/kT} + 1} \tag{2.3}$$

where E_{fv} is the quasi-Fermi energy in the valence band. All energies are measured from the bottom of the corresponding band.

Let $\rho_c(E)$ be the density of states in the conduction band and $\rho_v(E)$ be that of the valence band. A photon can be absorbed to create an electron of energy E_c and a hole of energy E_v. The absorption rate is given by

$$R_a = B\rho_c(E)\rho_v(E)\,[1-f_c(E_c)][1-f_v(E_v)] \tag{2.4}$$

where B is the transition probability, $1-f_c(E_c)$ and $1-f_v(E_v)$ represent the probabilities that the electron and hole states of energy E_c and E_v are not occupied. On the other hand, the stimulated emission rate of photons is given by

$$R_e = B\rho_c(E)\rho_v(E)\,f_c(E_c)f_v(E_v) \tag{2.5}$$

Thus, the condition for a net optical gain is that the stimulated emission rate exceeds the absorption rate or

$$R_e > R_a \tag{2.6}$$

Using Equations (2.4) and (2.5), this condition becomes

$$f_c(E_c)+f_v(E_v)>1 \tag{2.7}$$

Substituting the expressions for $f_c(E_c)$ and $f_v(E_v)$ into Equation (2.7), we have

$$E_{fc} + E_{fv} > E_c + E_v \tag{2.8}$$

Adding E_g to both sides of the Equation (2.8), it becomes

$$E_{fc} + E_{fv} + E_g > E_c + E_v + E_g = h\nu \tag{2.9}$$

The left side of the inequality is the quasi-Fermi level separation and the right side is the photon energy $h\nu$. Equation (2.9) states that the quasi-Fermi level separation of the conduction band and valence band must exceed the bandgap energy of the semiconductor in order to have a net optical gain. This is a necessary condition for laser action.

2.1.4 Modal confinement [21]

The radiation emitted by the gain medium must be confined in the active region by a waveguide. In a heterostructure semiconductor laser, the electric field confinement in the direction perpendicular to the junction plane occurred through dielectric waveguiding. This mechanism is often referred to as index guiding since the refractive index step (shown in Figure 2.3 (b))

between the active and cladding layers is responsible for the mode confinement through total internal reflection at the interfaces.

The electric field of an electromagnetic wave propagating in the z-direction along a waveguide is determined by the following equation:

$$(\frac{\partial^2}{\partial x^2}+\frac{\partial^2}{\partial y^2}+\frac{\partial^2}{\partial z^2})\ \vec{E}\,(x,y,z)+\varepsilon(x,y)k_0^{\,2}\vec{E}\,(x,y,z)=0 \qquad (2.10)$$

Where $\vec{E}\,(x,y,z)$ is the electric field, $\varepsilon(x,y)$ is the dielectric constant and k_0 is the wave vector in vacuum. Here, we assume that the dielectric constant is independent of z.

One approach to solve the above equation is based on the effective-index approximation. This approach can be applied to the case in which the dielectric constant varies very slowly in the lateral x direction along the junction plane compared to its variation in the transverse y direction (perpendicular to the junction plane). Thus the electric field can be assumed to be

$$\vec{E}(x,y,z)=\vec{e}\,\Phi(y)\Psi(x)\exp(i\beta z) \qquad (2.11)$$

where z is the direction of propagation, β is the propagation constant of the mode and $\vec{e}$ is a unit vector in the direction of the polarization.

By substituting $\bar{E}$ into Equation (2.10), we have

$$\frac{1}{\Psi}\frac{\partial^2\Psi(x)}{\partial x^2}+\frac{1}{\Phi}\frac{\partial^2\Phi}{\partial y^2}+[\varepsilon(x,y)k_0^2-\beta^2]=0 \qquad (2.12)$$

To obtain the solution for the above equations, one must know the distribution of the dielectric constant $\varepsilon(x,y)$ or the refractive index for each layer in the structure.

The loss or gain effect is generally treated as a small perturbation to the eigenvalue problem. This is appropriate for heterostructure semiconductor lasers since the mode confinement in the y direction is mainly caused by the index step at the heterostructure interfaces. The dielectric constant ε is of the form

$$\varepsilon(x,y)= \mu^2_b (y)+\Delta\varepsilon(x) \qquad (2.13)$$

where $\mu_b(y)$ is the structural refractive index whose variation is on the order of 0.1. The small perturbation, $\Delta\varepsilon(x)$, caused by the loss and the contribution of external pumping is on the order of 10^{-3}.

By separating the variables in Equation 2.12, the y-component satisfies the following eigenvalue equation

$$\frac{d^2\Phi}{dy^2}+[k_0^2\mu_b^2(y)-\beta_{eff}^2]\Phi=0 \qquad (2.14)$$

where β_{eff} is the effective propagation constant and can be determined by solving Equation (2.14). The solution to Equation (2.14) gives the transverse eigenmodes for the structure. In a slab waveguide, it is found that two sets of modes can exist, the TE modes and the TM modes, characterized according to their polarization. For the TE modes, the electric field E is polarized along the heterojunction plane, i.e., the polarization vector in Equation (2.11) is along the x axis. For the TM modes, the magnetic field H is polarized along the x axis.

For a heterojunction laser, the modal gain for a specific optical mode is given by

$$\gamma_{mode}(\omega) = \gamma(\omega)\Gamma \tag{2.15}$$

where $\gamma(\omega)$ is the gain of the bulk material, which is the gain when the entire optical mode is confined in the active layer and Γ is the overlapping factor of the eigenmode with the active layer, defined as

$$\Gamma = \frac{\int_{thickness} \Phi^2(y)dy}{\int_{-\infty}^{\infty} \Phi^2(y)dy} \tag{2.16}$$

Typically, the overlapping factor is on the order of a few percent for quantum-well lasers.

2.2 Development of II-VI compound semiconductor laser diode

2.2.1 Early ZnSe-based II-VI laser diodes

The II-VI semiconductor materials have long been studied for laser applications. Compared to the III-V materials, the II-VI materials, such as ZnSe, have much smaller cohesive energy. They are softer, more easily damaged and form many kinds of defects. Doping is also difficult. In 1987, Ohkawa et al[22] showed that chlorine is an excellent n-type dopant in MBE growth, with dopant levels about 10^{19} cm^{-3} routinely achievable.

P-type doping to ZnSe was extremely difficult to achieve. After years of research, a breakthrough finally came in 1991, when Ohkawa et al[23] and Park et al[24] showed that an RF plasma source could be used to produce excited nitrogen atom which would be incorporated in the ZnSe epilayer. A p-dopant level of 2×10^{18} cm^{-3} was obtained which is high enough for making a p-n junction devices. Soon after that, the first ZnSe-based laser diode (LD) was fabricated at 3M[8]. Even though the laser operated only for a few seconds, the success opened a new era for II-VI compound diode laser research.

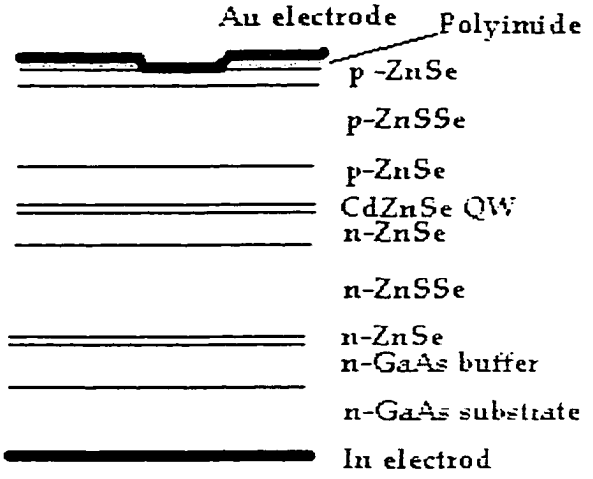

Figure 2.6 The layer structure of the first ZnSe-based laser diode [8]

Figure 2.6 shows the layer structure of the first II-VI LD. The active layer was a 10-nm-thick $Zn_{0.8}Cd_{0.2}Se$. The p-ZnSe and n-ZnSe layers served as the barriers for confining carriers and as the core of the waveguide for mode confinement. The cladding layers were two thick $ZnS_{0.07}Se_{0.93}$ layers. The first LD is a gain-guided laser with 20-micron-wide gold electrode buried in an insulator layer.

Other groups have tried a variety of structures similar to that of the first LD[25]-[29], and found no significant improvement in the laser properties.

In the early days of II-VI laser diode, the ZnSe layers in the laser were generally about 0.5 μm thick, which is much larger than the critical thickness. Because of the lattice constant mismatch (about 0.3%) between

the ZnSe and GaAs substrate, high density of dislocations (above 10^6 cm^{-2}) were found at the interface which may have contributed to the short lifetime of the laser diode.

Another problem of the first generation II-VI laser diode is the difficulty in making Ohmic contact between the p-doped layers and metal electrode. The non-Ohmic contact behavior raises the turn-on voltage for the laser diode to about 20-30 V, with most of the potential drop occurring at the p-side contact. The resistive barrier generates a large amount of heat during the operation of LD and may also have contributed to the degradation of the laser.

In addition, the confinement for carriers and optical mode was insufficient. The bandgap energy difference between the ZnCdSe and ZnSe was only about 250 meV. The valence band offset was too small to provide effective carrier confinement. As a result, the first laser could be only operated at 77 K.

With all the above mentioned problems, the device lifetime was rather short, in the range of several seconds to several minutes.

2.2.2 Improved structure based on ZnMgSSe

The use of lattice-matched materials improved the quality of laser diodes. The ZnMgSSe quaternary material was first introduced at the North American Philips laboratories [30,31] and at SONY [32]-[35] to improve the confinement of carrier and optical mode. ZnMgSSe has much a wider range of the bandgap energy from 2.78-4.5 eV. The ZnSe-ZnMgSSe interface is expected to exhibit a type-I heterostructure [36] with a valence band discontinuity of about 50% of the bandgap energy difference. In addition, from a reflection-spectrum measurement [37], it has been shown the refractive index of ZnMgSSe is smaller than that of ZnSe. Thus a ZnSe layer sandwiched between two ZnMgSSe layers can provide optical confinement and carrier confinement. Photo-pumped lasing in undoped Zn(S)Se-ZnMgSSe DH structures has been realized at temperatures up to 500K. This confirms that the ZnMgSSe forms a type-I heterostructure with ZnSe and has a refractive index smaller than that of ZnSe.

And more importantly, ZnMgSSe can be grown lattice matched to GaAs substrate. The use of ZnMgSSe as the cladding layers allows the use of ZnSSe, also lattice matched to GaAs, as the barriers.

The main problem is making an Ohmic contact to p-ZnSe. The valence band maximum of ZnSe is approximately 6.4 eV below the vacuum level and no metal has a work function larger than 5.6 eV. Therefore, there exists a large Schottky barrier between the metal and the p-type ZnSe. Traditionally, a solution to this problem is to alloy the contact metal with semiconductor, but this approach was not successful because the materials were unstable during thermal annealing. Another possible approach is to dope the semiconductor layer extremely heavily to promote tunneling. However this cannot be done because the p-doping level beyond 10^{18} cm^{-3} was not easily obtainable in ZnSe.

In order to make good p-type contact, an intermediate layer must be inserted between the metal and p-type ZnSe, so as to move the top of the valence band closer to the metal work function, as was done in the case of n-typed GaAs/Au contacts by using GaInAs[38]. In searching of a good contact layer to p-ZnSe, several materials have been experimented. ZnTe was a promising candidate for the intermediate layer because of its high valence band position and its ability of being p-doped to above 10^{19} cm^{-3}. To remove any problems produced by the valence band discontinuity between the ZnTe and ZnSe layers, a ZnTe-ZnSe superlattice structure in which the

width of the ZnSe and ZnTe layers is gradually varied was introduced to simulate an alloy of continually varying composition[39]. It has been shown to have low operating voltage[40]. This idea has been adapted by the SONY group, who have used narrow ZnTe quantum wells of varying thickness between ZnSe barriers. By varying the well width in the region of strong band bending, it is possible to produce a structure in which all the well levels are at the same energy to enhance tunneling[41]. On the other hand, the metal electrode has been improved by using Au-Pt-Pd[42]. It is found that the specific contact resistance to p-type ZnTe as low as 5×10^{-6} Ohm cm^{-2} has been achieved.

With these improved contact layer and metal electrode, the threshold voltage for the II-VI laser diode has been dramatically reduce to about 4 V,[43,44] which is only about one fifth of that of the early lasers.

In 1996, SONY demonstrated a 100 hour blue-green laser at room temperature under cw operation [13]. Figure 2.7 shows the schematic structure of the laser. Figure 2.7 (a) is the layer structure of the laser diode. ZnCdSe quantum well layer was embedded in ZnSSe guiding layers and ZnMgSSe cladding layers. The resonant tunneling ZnSe-ZnTe multi-

quantum-well structure (shown in (b)) was introduced to enhance the tunneling of holes. By optimizing the growth condition, the density of defects was smaller than 3×10^{3} cm^{-2}.

The turn-on voltage of the laser fabricated by SONY is about 7 V. The operating voltage is about 11 V, which is too high for a commercial device. High operating voltage generates excessive heat in the contact layer, which is one of the causes of short device lifetime in II-VI laser diodes. Optimizing the contact structure by reducing the thicknessof ZnTe layer to 4 nm was shown to reduce the operating voltage to 4.2 V, and much longer electrode lifetime of 1000 hours[45] and device lifetime of 400 hours[46] were achieved.

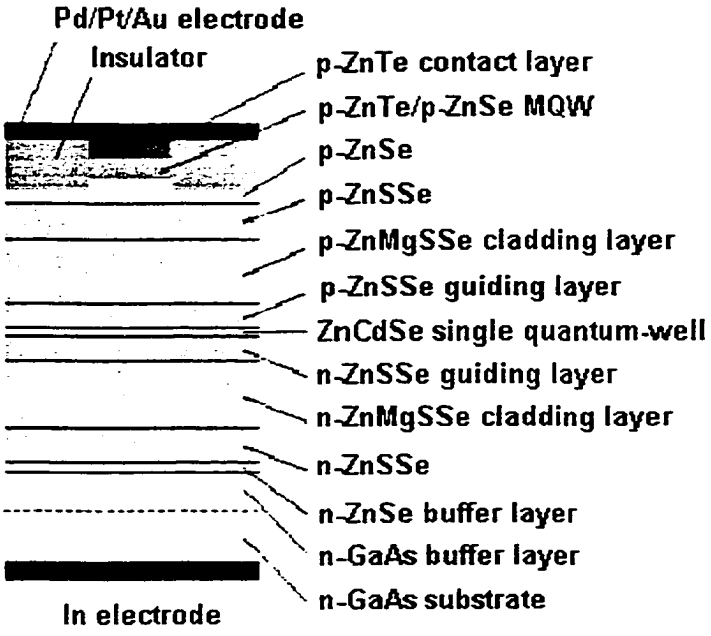

(a) Layer structure of the SONY LD

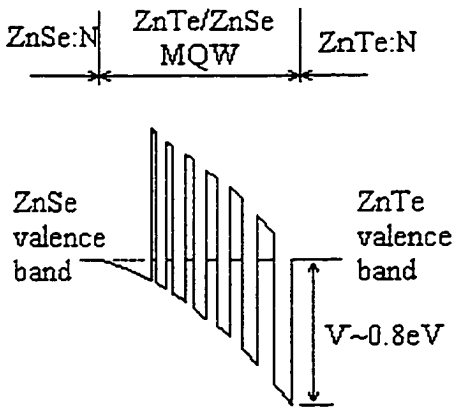

(b) the tunneling ZnSe-ZnTe MQW structure

Figure 2.7 Schematic structure of the SONY laser diode. (a) The layer structure of the laser diode. [13] (b) The ZnSe-ZnTe multi-quantum-well structure used to enhance the tunneling effect [42].

2.2.3 Challenges

One of the major obstacles limiting the lifetime of ZnCdSe/ZnSSe/ZnMgSSe devices grown on GaAs substrate is the pre-existing defects and the formation of dislocation networks in the active region due to recombination-enhanced defect migration. It is reported that the degradation of ZnSe-based II-VI laser diodes grown on GaAs substrate originates at pre-existing defects (mainly stacking faults) and propagates by the formation of <100> dark line defects (DLDs) in or near the active layer [47]-[56]. The formation of DLDs is observed in both electrical and optical injection devices. In the initial state of degradation, DLDs develop along the pathways of dark mobile defects, which originate from pre-existing defects. With time, the DLDs grow, branch, and broaden forming large areas of nonradiative recombination centers. Spatially resolved cathodoluminescence study shows that nonradiative recombination processes associated with DLDs are thermally activated [57].

In the past years, the research had been concentrated to reduce the density of stacking faults and related threading dislocations originated in the vicinity of the II-VI/III-V interface. It was shown [58][59] that growing a GaAs buffer layer on a GaAs substrate and exposure to a zinc beam before growth of

II-VI compound layers on the As stabilizes surface of the GaAs buffer layer have greatly improved the II-VI/III-V interface and reduced the density of stacking fault. As a result, device lifetime of II-VI laser diodes has been lengthened to a few hundred hours.

2.3 ZnCdMgSe material system

The structures and devices introduced above and widely studied so far are grown on GaAs substrates. The presence of strain in the active layer and the formation of misfit dislocations in the contact layer region due to the relaxation of the very large lattice-mismatch between ZnTe and the rest of the structure are likely sources of degradation of these devices. Therefore it is of interest to explore other wide bandgap II-VI materials that may be used to design entirely lattice-matched structures that also meet the band structure requirements of this complex device.

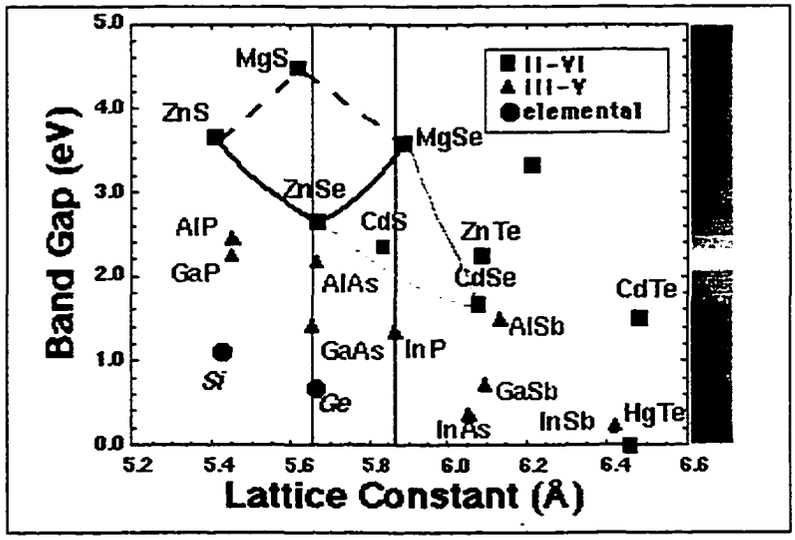

Figure 2.8 Bandgap energy versus lattice constant.

As seen in Fig. 2.8, a wide range of ternary and quaternary compositions of the (Zn,Cd)(Se,Te), (Zn,Cd,Mg)Se and (Zn,Cd,Mn)Se systems can be grown lattice matched to InP. Thus the use of InP as the substrate material makes it

possible to select among a set of new II-VI quaternary and ternary materials for the quantum well and barrier layers that can be all lattice-matched to the substrates. This offers great promise in terms of improved crystalline quality and reliability over the II-VI materials that have previously been used to fabricate visible lasers. The absence of strain also allows the fabrication of multiple quantum well lasers from these materials without being limited by the critical thickness. In addition, the room temperature bandgap for the ZnCdMgSe quaternary material ranges from 2.1 eV to well over 3 eV. Thus, in lattice-matched ZnCdSe/ZnCdMgSe quantum well structures, by controlling the thickness of the quantum well, the emission wavelength can be made to vary over a wide spectral range from orange to blue[19]. By changing the composition of the quantum-well layer, thus introducing some strain, on the order of 1%, in the quantum well, the emission wavelength can extend to red. Another feature of these structures grown on InP substrates is that it also allows the growth of a symmetrically strained [60][61] ZnSe/ZnTe superlattice or lattice-matched ZnSeTe alloys that may be easily doped p-type for Ohmic contact without introducing defects due to lattice-mismatch.

Recently, a material degradation study on the ZnCdSe/ZnCdMgSe quantum-well structures grown on InP shows no sign of the formation of DLDs in the active layer [62]. In that study, laser samples with and without strain in the quantum-well layer were irradiated by a strong electron beam and cathodoluminescence technique was used to observe the appearance of the DLDs. It has been shown that DLDs are not present in the vicinity of the active layer in both samples.

To summarize, the ZnCdSe/ZnCdMgSe material grown on InP has the following features:

(a) Emitting in the entire visible spectrum from red to blue.

(b) Lattice-matched material for better crystal quality.

(c) Freedom from the formation of DLDs in the active layer.

Chapter 3 Photopumping experiment on ZnCdSe/ZnCdMgSe quantum-well lasers

We have carried out a series of photo-pumping experiments and achieved laser action in ZnCdSe/ZnCdMgSe quantum-well lasers grown on InP. Using different thicknesses and/or composition of the quantum well, lasers emitting in red, green and blue have been demonstrated.

3.1. ZnCdMgSe materials

By using ZnCdMgSe as the cladding and waveguiding layers and ZnCdSe as the active layer, we design lattice-matched or pseudomorphic quantum-well structures with emission ranging from blue to orange. With 1.2% compressive strain in the quantum well, the emission wavelength has been extended to red.

The materials were grown by Molecular Beam Epitaxy (MBE) in Professor Maria Tamargo's laboratory at City College. The initial low temperature photoluminescence experiments were also carried out there.

A typical quantum-well structure consists of a thin(<10 nm) layer of smaller bandgap material sandwiched between two layers of larger bandgap materials. The discontinuity of energy bands in the conduction and valence bands results in a potential barrier that confines the carriers. The potential well's thickness is typically less than 10 nm.

The bandgap discontinuity in the conduction band and valence band forms the energy barriers for the electrons and holes. In the GaAs/AlGaAs quantum-wells, the ratio of the bandgap offsets in the conduction band and valence band is about 3:2. In the II-VI semiconductor system, the reported values are quite different for different material combination. Some reported a very small conduction band offset ($\Delta E_c \approx$ 6 meV for the $ZnSe/ZnS_{0.18}Se_{0.82}$ heterojunction reported by M. Lomascolo et al[63], $\Delta E_c/\Delta E_g \approx 0.1$ for the $ZnSe/Zn_{1-x}Mg_xS_ySe_{1-y}$ heterojunction reported by K. Shahzad et al[64], $\Delta E_c/\Delta E_v$=8/92 for the ZnS/ZnSe heterojunction reported by R. Cingolani et al[65]). Others reported larger conduction band offset ($\Delta E_c/\Delta E_g$=0.4 for the ZnSe/ZnMgSSe heterojunction reported by T. Miyajima at al[66], $\Delta E_v/\Delta E_g$=0.3 for the CdTe/(CdMn)Te heterojunction reported by W. Ossau et al[67]). To provide effective confinement of the electrons and holes, the energy barriers of the quantum well must be considerably larger than the thermal energy at room temperature (kT= 25 meV). Ishibashi[68] further estimated that the total bandgap energy difference between the active layer and the cladding layer should be greater or equal to 350 meV to have a low threshold laser diode.

A stand-alone quantum well is not an effective waveguide because the layer thickness is much smaller than the wavelength of light waves in the materials. To improve the confinement of the light wave propagating in the active region, a waveguide layer was inserted between the active layer and the cladding layer.

Figure 3.1 (a) shows the layer structure of the quantum-well laser based on ZnCdSe/ZnCdMgSe grown on InP. The light-emitting region is a 4 nm $Zn_{1-x}Cd_xSe$ ($x \approx 0.5$) single quantum well with a nominal bandgap of 2.2 eV. The quantum well is embedded in a waveguide which consists of two 0.2-micron $Zn_xCd_yMg_{1-x-y}Se$ layers whose nominal bandgap energy varied from 2.7 eV (x=0.37, y=0.27) to 3.0 eV (x=0.27, y=0.20). The cladding layers are two 0.5-micron-thick quaternaries $Zn_xCd_yMg_{1-x-y}Se$ with a nominal bandgap of 3.0 eV. A 10-nm ZnSe cap layer is used to protect the magnesium in the top cladding layer from oxidizing. The bandgap energy profile of the laser was shown in Figure 3.1 (b). The proposed refractive-index profile of the waveguide structure is shown in Figure 3.1(c). In semiconductor materials, the refractive index decreases with increasing

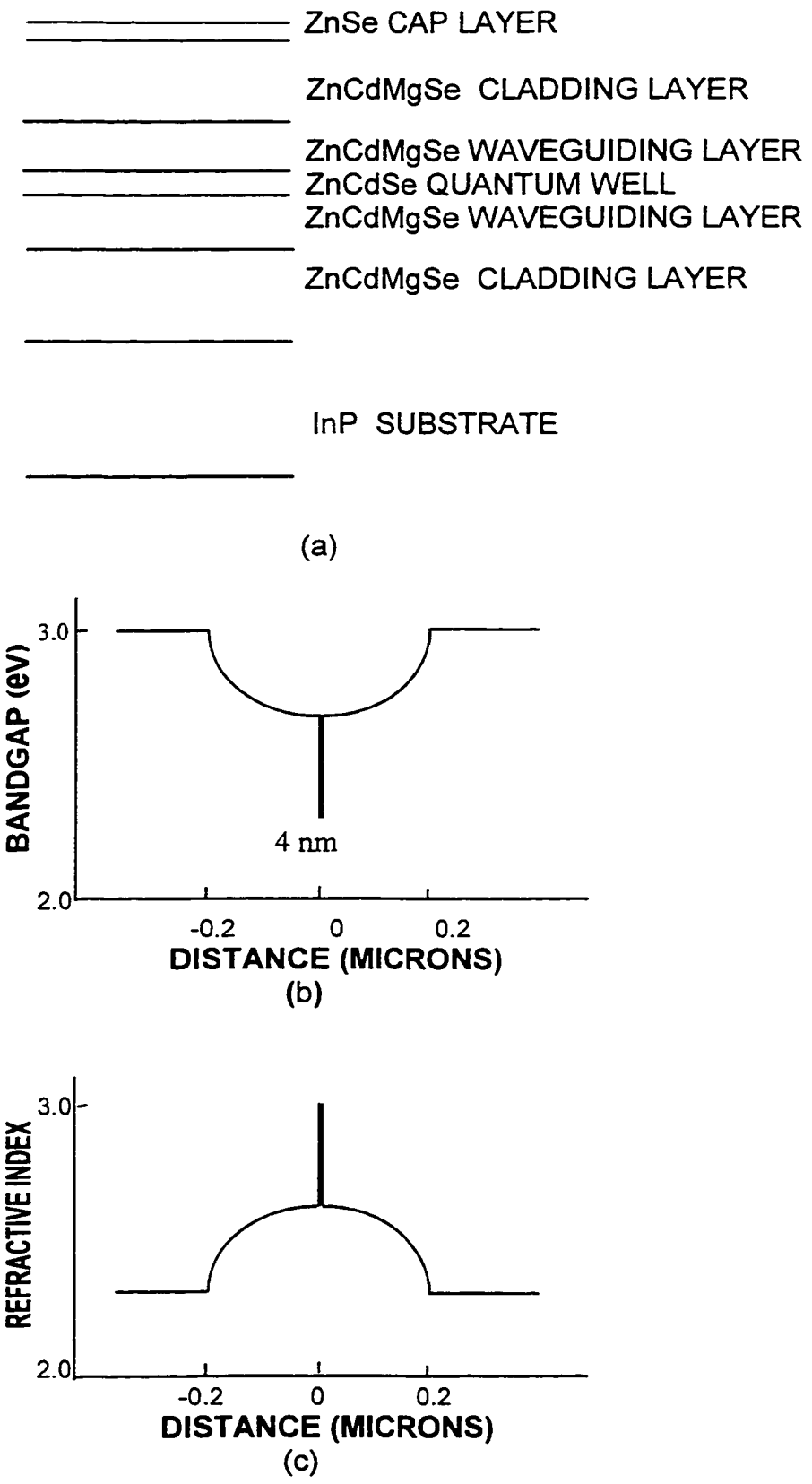

Figure 3.1. (a) Quantum-well laser structure, (b) bandgap profile, and (c) refractive index profile of a ZnCdSe/ZnCdMgSe quantum-well structure grown on InP.

bandgap energy. Thus, the layer structure that produces a bandgap-energy profile for carrier confinement also creates a waveguide for optical confinement.

3.2 Photoluminescence measurements

Photoluminescence is a useful tool for determining the emission wavelength of the material and, when the material parameters are known, the approximate carrier concentrations as well. For example, in the case of bulk GaAs, the carrier concentration can be estimated from the position of the peak energy and/or the width of the emitted radiation [72].

The characterization of ternary material ZnCdSe and quaternary material ZnCdMgSe grown on InP substrate was done by low temperature photoluminescence at City College. Excellent layer quality for ternary material is evident from the extremely narrow peak (10 meV) and efficient photoluminescence bandedge emission and the near absence of defect-related deep level emission.[70] The quaternary material layers encompass a wide range of bandgap, from 2.18 eV to above 3.5 eV, as shown in Figure 3.2.

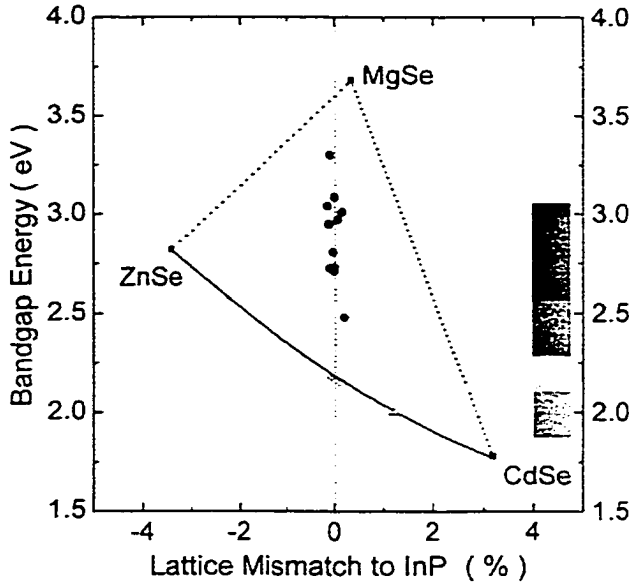

Figure 3.2 Bandgap energy (based on the low-temperature photoluminescence measurement) and lattice constant of ZnCdSe and ZnCdMgSe materials.

The photoluminescence spectra[71] of one of the laser structures, Sample 382, are shown in Figure 3.3. The structure of the sample was similar to that described in previous section (Figure 3.1) but with a step refractive index profile. The measurements were made using the 325-nm output of a He-Cd laser as the excitation source and a double spectrometer and photomultiplier tube as detector. The photoluminescence was measured on the as-grown wafer (trace a) and on a sample of the wafer that has been etched with dilute Bromine-Methanol solution to remove about 0.8 microns from the surface (trace b). The strongest emission observed from the as-grown sample is at 405 nm (peak 1) and corresponds to the bandgap energy of the top cladding quaternary layer. Since most of the light is absorbed near the surface, the

emission from the underlying layers is expected to be weak. In fact, weak emissions are also seen at 420 and 490 nm, the wavelength expected from recombination at the bottom of the graded waveguide region and the quantum well, respectively. Upon etching away most of the 1-micron-thick cladding layer (trace b) the intensities of the two lower energy peaks, in particular that attributed to the quantum well emission (peak 3), increase dramatically. This clearly confirms the presence of the quantum well and waveguiding layers.

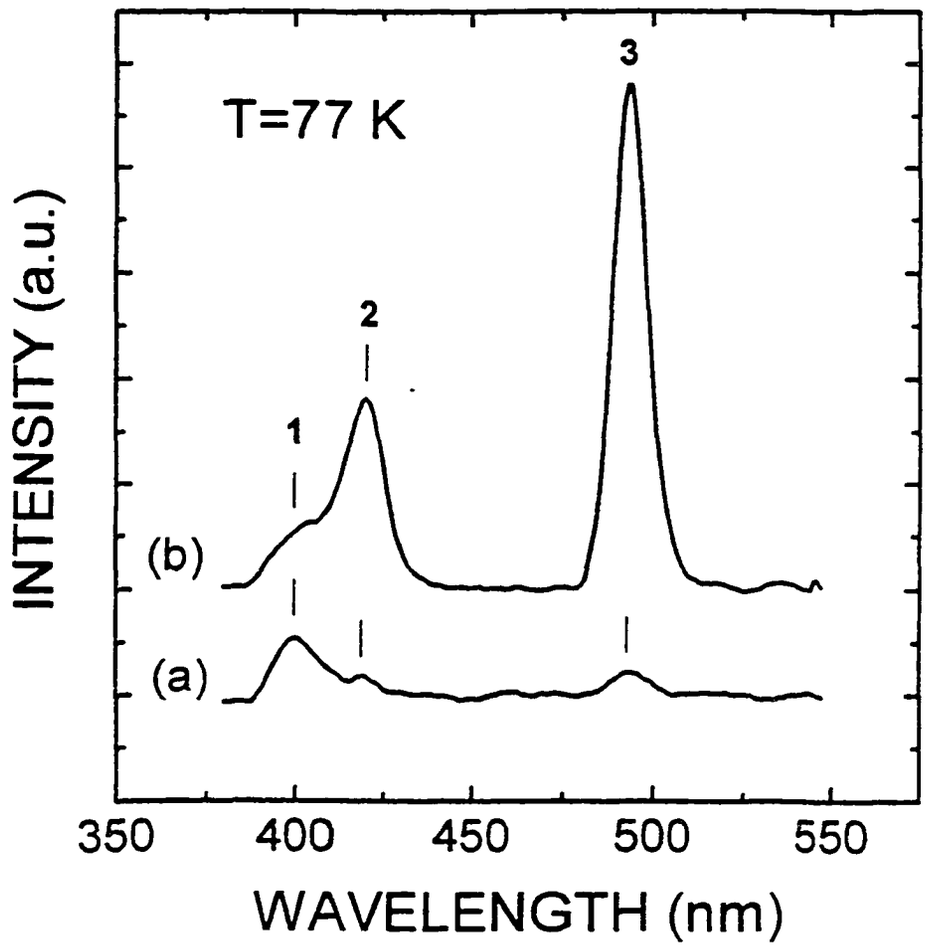

Figure 3.3 Low-temperature photoluminescence spectra of sample 382. (a) Spectrum for the as-grown sample. (b) Spectrum with most of the top layer etched.

3.3 Waveguide design

The design of the waveguide depends on the knowledge of refractive index of the materials. Since at this stage, the material parameters for the quaternary material ZnCdMgSe grown on InP are still largely unknown, the waveguide design is based on the published data of refractive indices as a function of material composition for ZnMgSSe grown on GaAs. The eigenmode of the electromagnetic wave in the waveguide was calculated by a computer program, which is based on the theory described in Chapter 2.1.4. The results are shown in Figures 3.4 and 3.5.

Both graded-index (with gradually changing composition of the material, thus the bandgap energy and refractive index) and step-index (with step-like variation in the material composition) waveguides have been used. The refractive-index profile of the waveguide structure was constructed by assuming a refractive index vs bandgap energy relation found in the ZnMgSSe/GaAs system.[72] Figure 3.4 shows the profile of the step-index waveguide and the calculated intensity distribution of the eigenmode. The structure used in the calculation has a 4-nm-thick quantum well embedded in 0.2-micron-thick waveguiding layers and 0.5-micron-thick cladding layers. The optical confinement factor Γ for the fundamental transverse wave is

1.35%. By reducing the thickness of the waveguiding layer to 0.1-micron, the overlapping of the fundamental transverse wave with the quantum well increases to 1.79% and 2.40% for step-index profile and graded-index profile respectively (shown in Figure 3.5). The calculation shows that the graded structure provides better optical confinement or larger value of Γ.

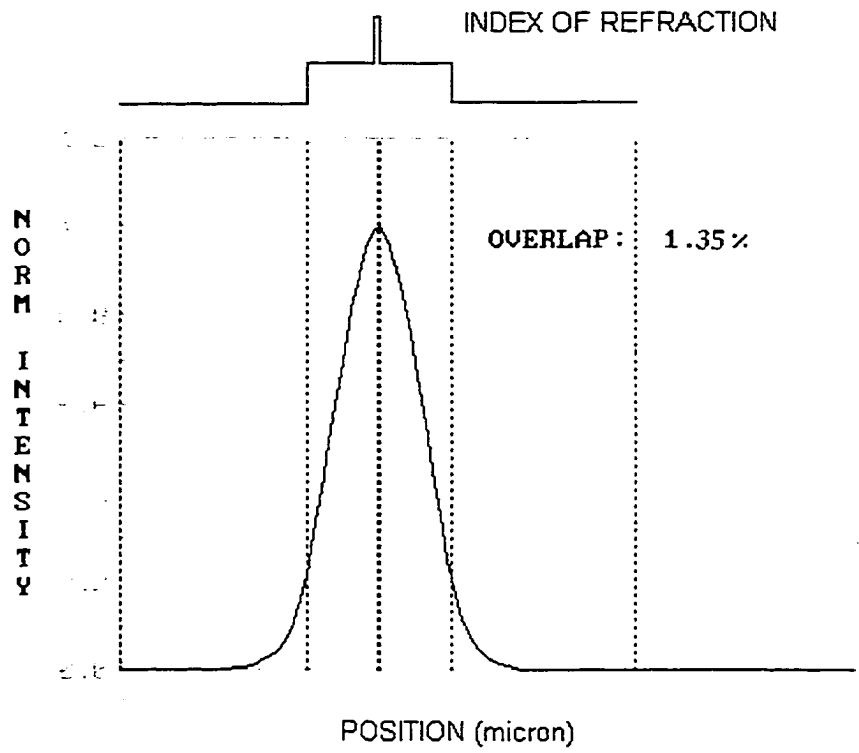

Figure 3.4 TE mode with a step-index profile. The quantum well layer is 4-nm thick, the waveguiding layer is 0.2-microns thick and the cladding layer is 0.5-microns thick. The upper plot is the refractive-index profile. The lower plot is the transverse-electric mode of the electromagnetic wave in the waveguide.

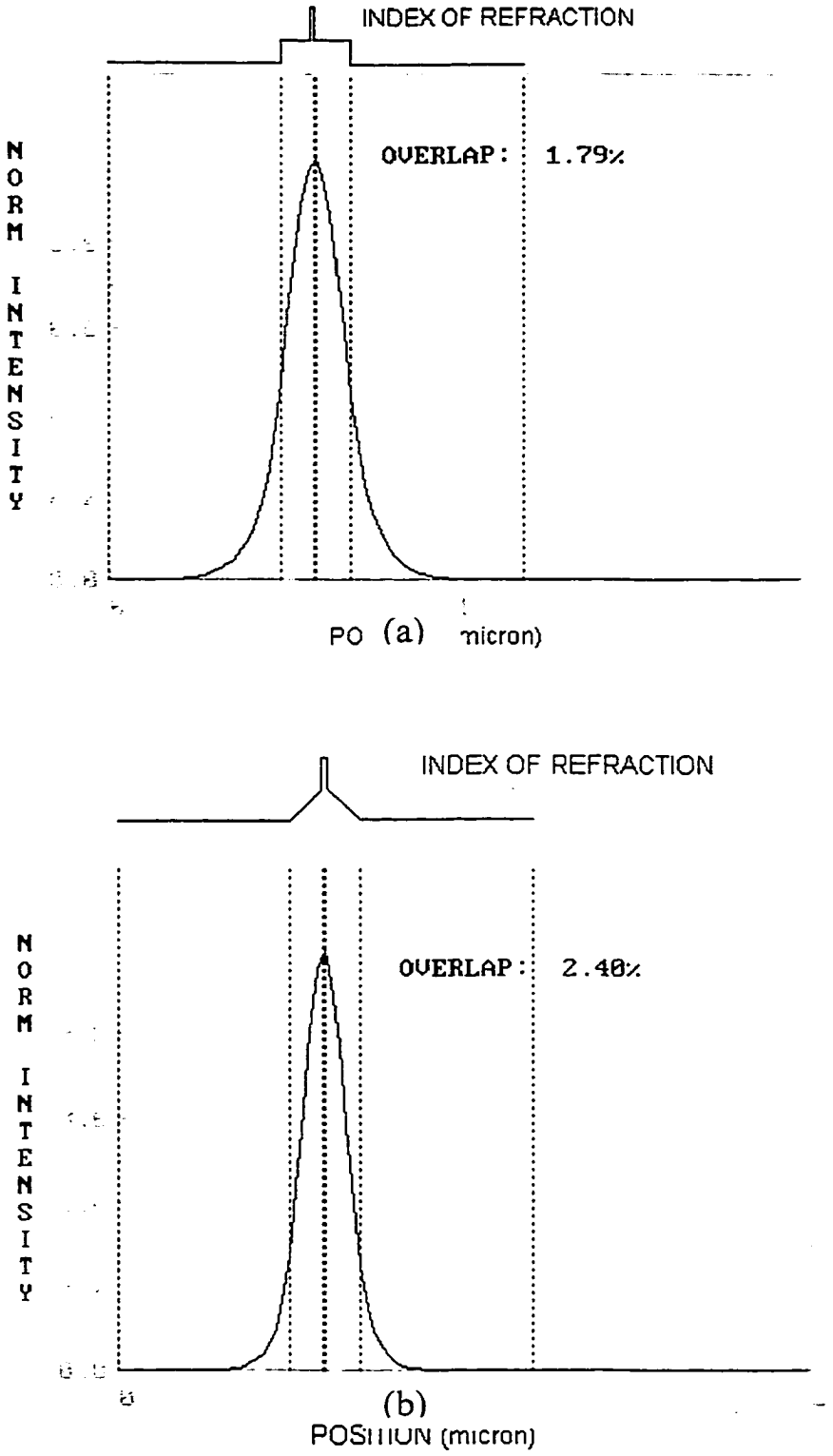

Figure 3.5 TE mode with (a) step-index profile and (b) graded-index profile by reducing the thickness of the waveguiding layer. The quantum well layer is 4-nm thick, the waveguiding layer is 0.1-microns thick and the cladding layer is 0.5-microns thick.

The size of the guided mode inside the waveguide can be inferred from the width of the laser beam in the far field. The far-field measurement was done by placing the laser sample in the center of a circle and moving the detector along the circular path in the plane perpendicular to the junction plane.

Figures 3.6 and 3.7 show the far-field beam intensity profiles for Samples 382 and 383. The structural parameters of these samples are given in Table 3.1. Both samples have a step-index profile. The only difference of the laser structure between these samples is the quantum well thickness.

Table 3.1 Structure parameters for Samples 382 and 383

Sample number	Bandgap energy and thickness of the cladding layer		Bandgap energy and thickness of the waveguiding layer		Thickness of the quantum well layer	Laser wave-length
382	2.95 eV	500 nm	2.7 eV	100 nm	4 nm	540 nm
	n=2.62*		n=2.86*			
383	2.95 eV	500 nm	2.7 eV	100 nm	2.8 nm	497 nm
	n=2.62*		n=2.86*			

* n is the estimated index of refraction.

The filled circles in Figures 3.6 and 3.7 are the experimental data. The solid lines show the best-fit Gaussian profiles given by

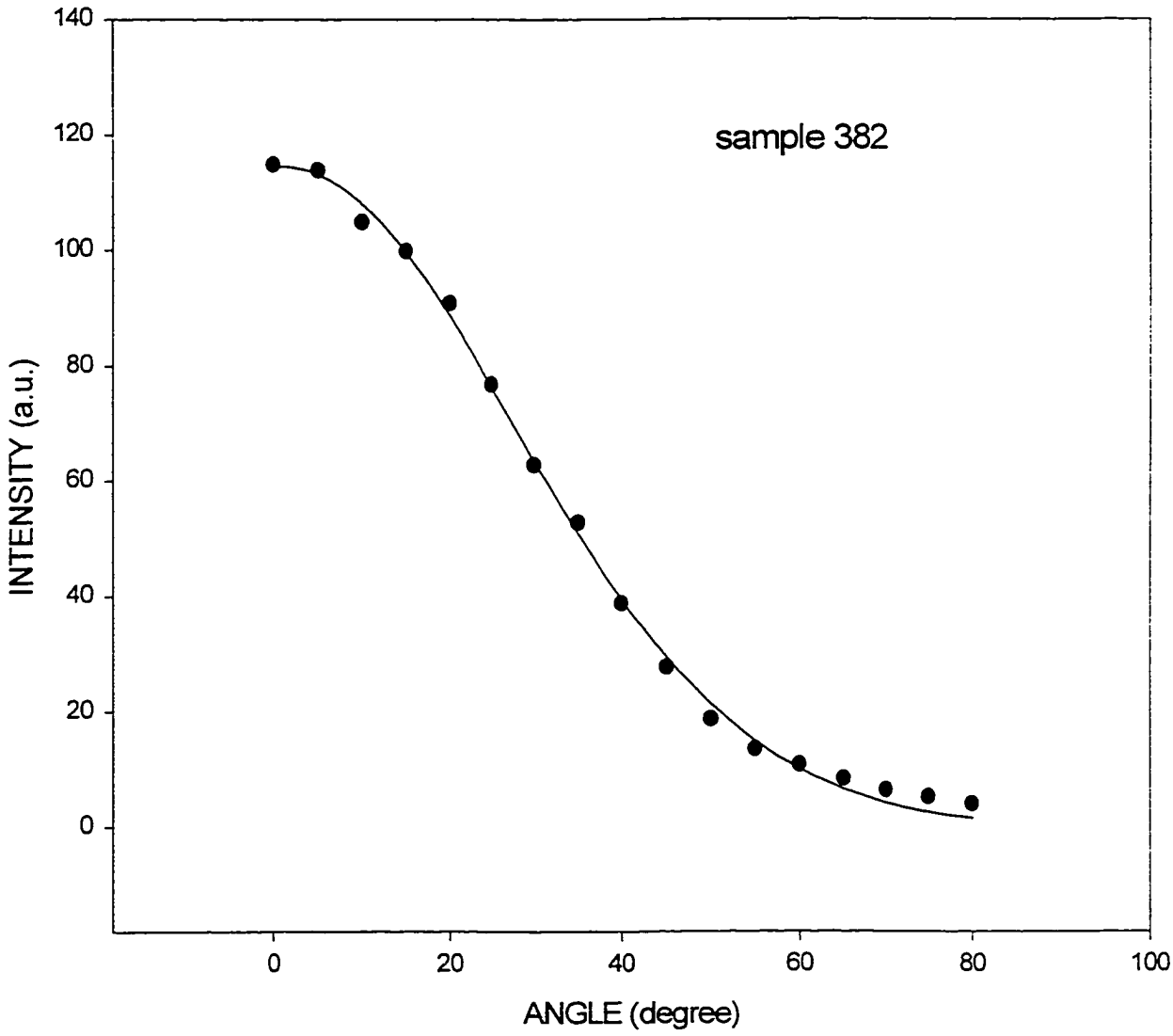

Figure 3.6 Far-field intensity profile of Sample 382. The filled circles are the experimental data. The solid line is a Gaussian profile $I(\theta) = 114.4\exp[-2(\frac{\theta - 0.8052}{53.71})^2]$

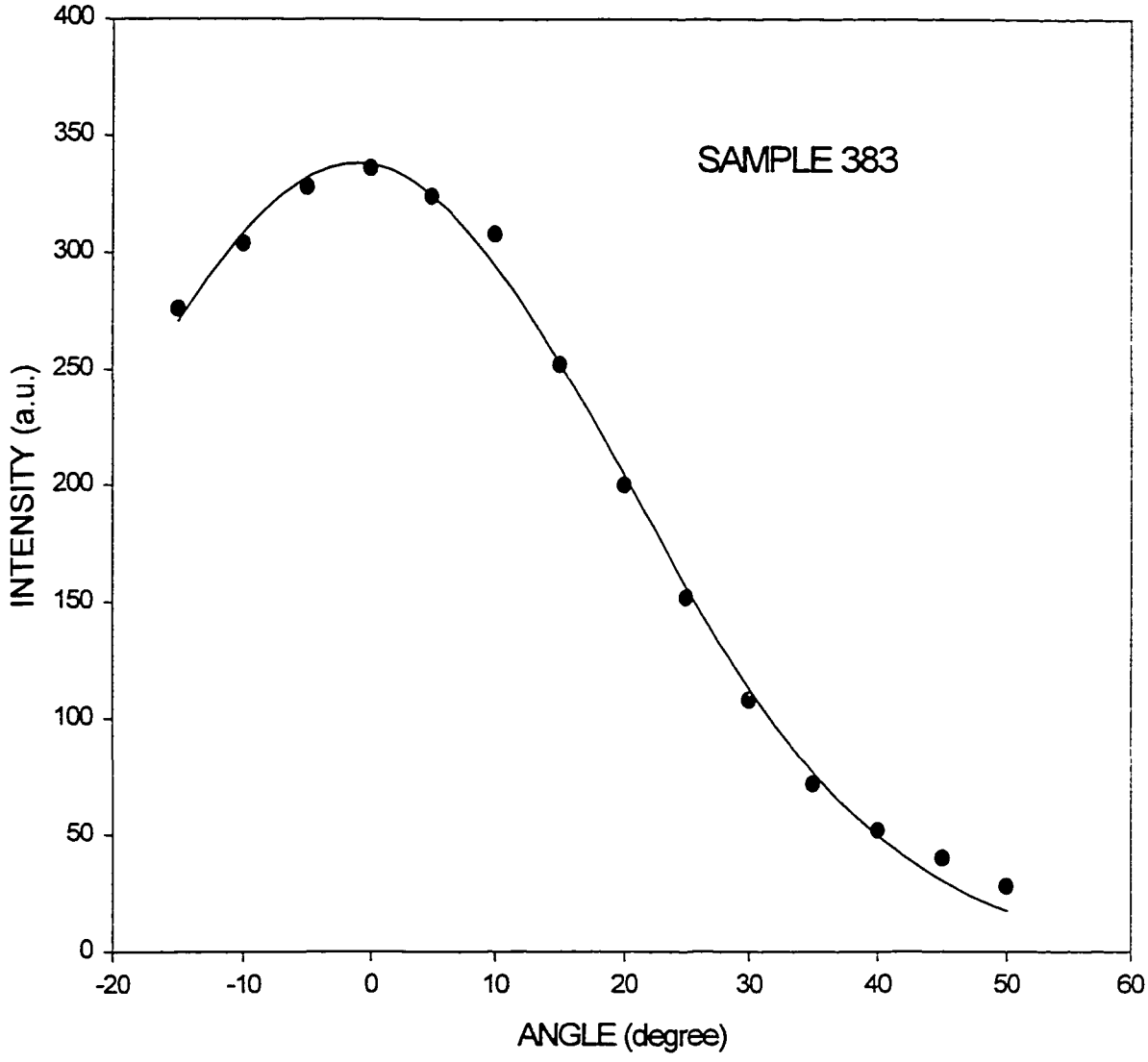

Figure 3.7 Far-field intensity profile of Sample 383. The filled circles are the experimental data. The solid line is the Gaussian profile

$$I(\theta) = 338.1 \exp[-2(\frac{\theta + 1.036}{41.91})^2]$$

$$I(\theta) = I_0 \exp[-2(\frac{\theta - \theta_0}{\Omega})^2] \quad (3.1)$$

Where I is the intensity, I_0 is the maximum intensity, θ_0 is the center of the beam and Ω is the beam width. The angular beam width of the far-field intensity profile at $1/e^2$ of the maximum is 53.71 degrees for Sample 382 and 41.91 degrees for Sample 383.

For a laser beam with Gaussian distribution in the intensity profile, the beam width of the far-field pattern is related to the beam width in the near-field pattern by

$$\Omega = \frac{\lambda}{\pi w n} \quad (3.2)$$

where Ω is the beam width in the far-field, λ is the wavelength, w is the beam width in the near-field, and n is the index of refraction.

Using Equation 3.2, the beam widths in the nearfield for Samples 382 and 383 are 0.18 micron and 0.21 micron, respectively. By using the estimated indices of refraction listed in Table 3.1, the calculated beam sizes inside the waveguide are 0.22 micron and 0.21 micron for Samples 382 and 383, respectively. Thus the calculation is in agreement with the experiment.

3.4 Photo-pumping experiments

We have carried out a series of photopumping experiments and have demonstrated laser action in ZnCdSe/ZnSe and ZnCdSe/ZnCdMgSe quantum-well lasers.

The experimental setup for photopumping is shown in Figure 3.8. A frequency-tripled Nd:YAG laser pumped dye laser was used as the pump source. The pulse width and repetition rate of the dye laser output was 7-ns and 20 Hz, respectively. To ensure the largest concentration of photo-generated carriers in the vicinity of quantum-well, the wavelength of the dye laser was tuned to 460 nm, corresponding to a photon energy near the bandgap of the bottom of the graded-index waveguide at room temperature. The sample was thinned to about 100-microns thickness and cleaved into 1-mm-wide bars for photopumping. The pump beam was focused onto the surface of the wafer to create a stripe-geometry excitation region along the (110) direction. A variable attenuator was used to control the pumping intensity. The edge emission of the laser bar was collected by a microscope objective and focused into an optical multichannel analyzer to analyze the spectral characteristics. A boxcar integrator was used to measure the pumping power and output power.

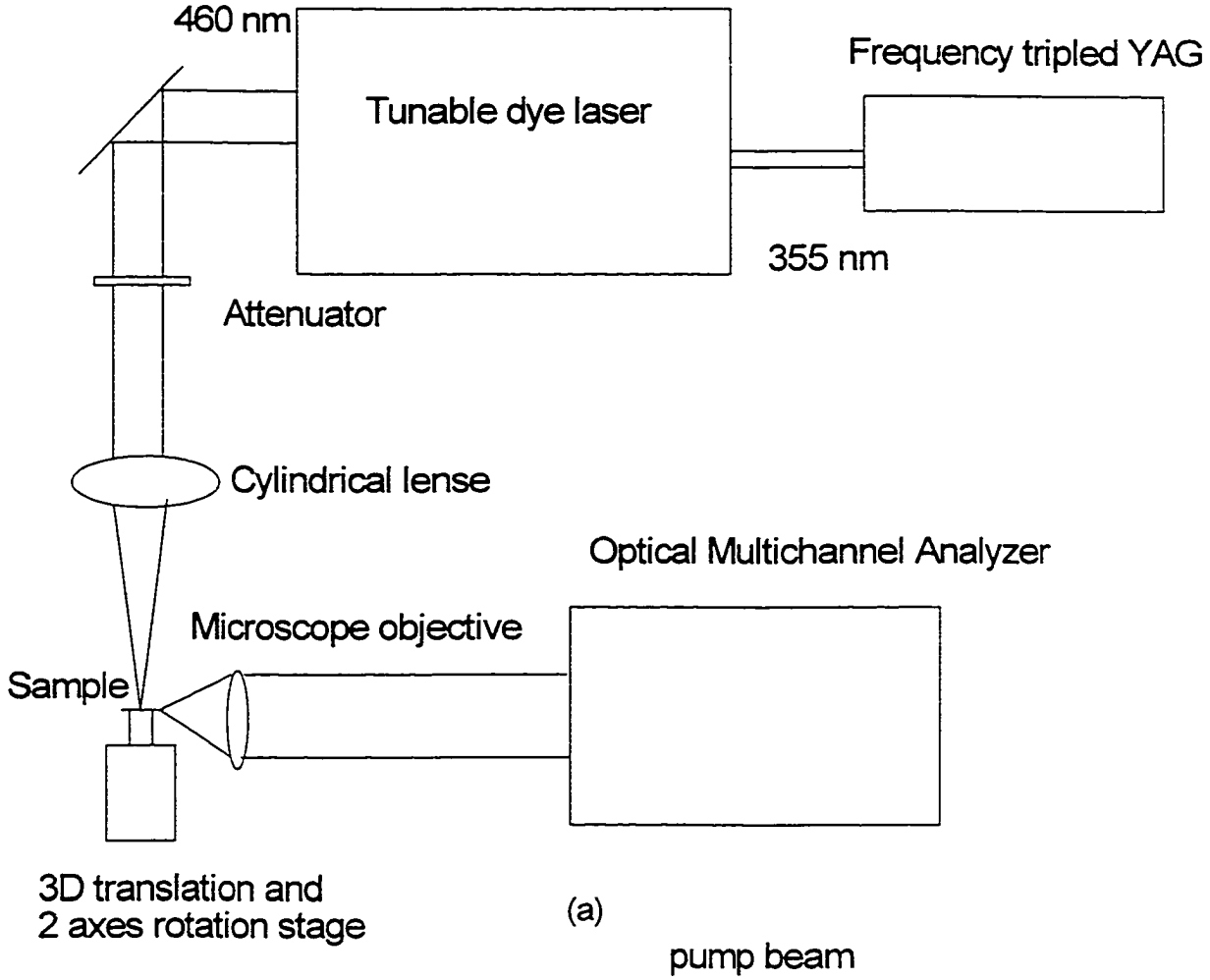

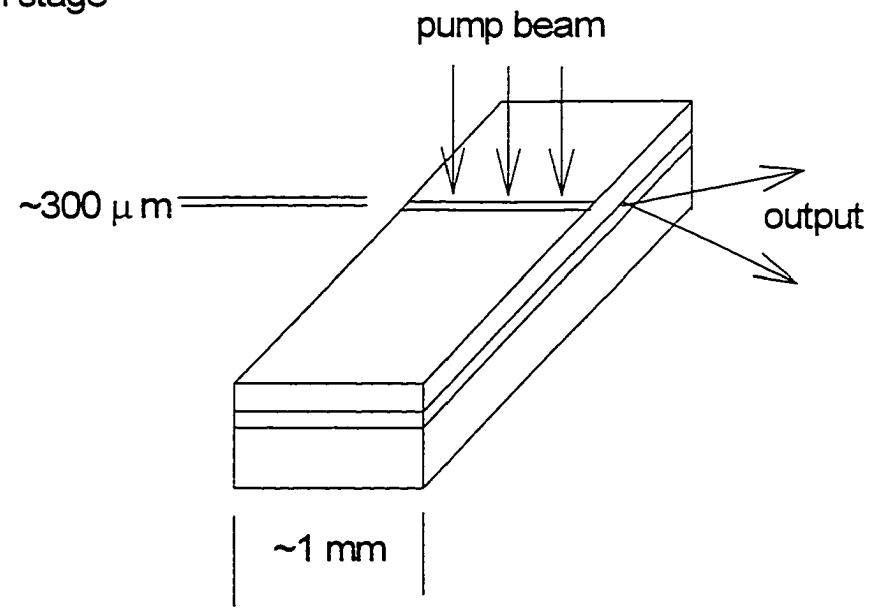

Figure 3.8 (a) Experimental setup for the photopumping experiment. (b) Pumping geometry on the chip

Figure 3.9 shows the output intensity from the single-quantum-well laser as a function of pumping intensity. The output vs input characteristics exhibited a clear transition from a slightly superlinear relation below the lasing threshold to a linear relation above the threshold. The threshold occurs at a pumping power density of 160 kW/cm^2.

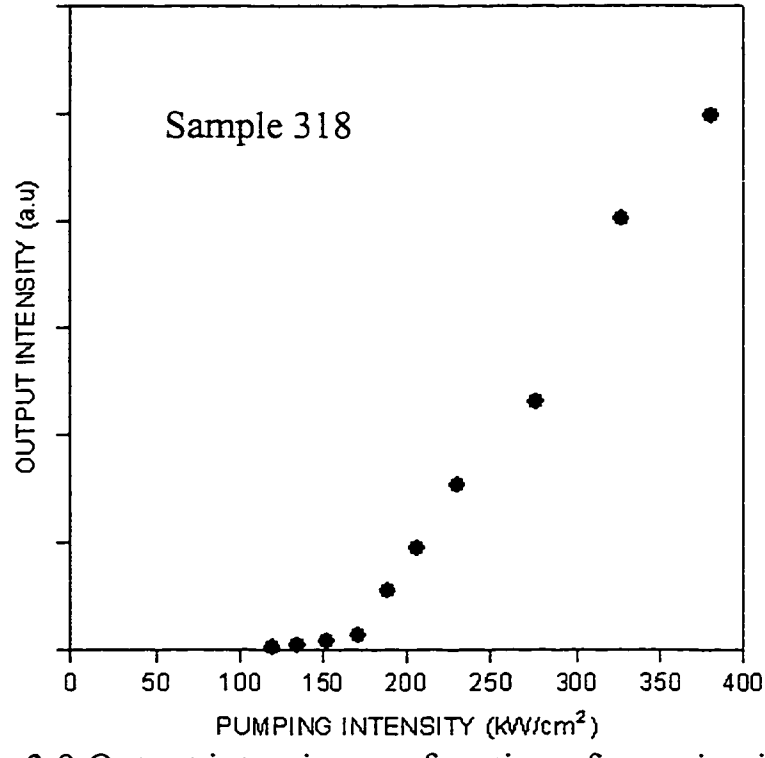

Figure 3.9 Output intensity as a function of pumping intensity

Shown in Figure 3.10 are the spectra of the edge emission below and above the lasing threshold. The onset of laser oscillation at 512 nm is accompanied by a narrowing of the spectrum. Both the turn-on characteristics of the power curve (Figure 3.9) and the width of the

stimulated emission line (Figure 3.10) are qualitatively very similar to the behavior of the ZnSe/ZnMgSSe lasers previously reported.[73]

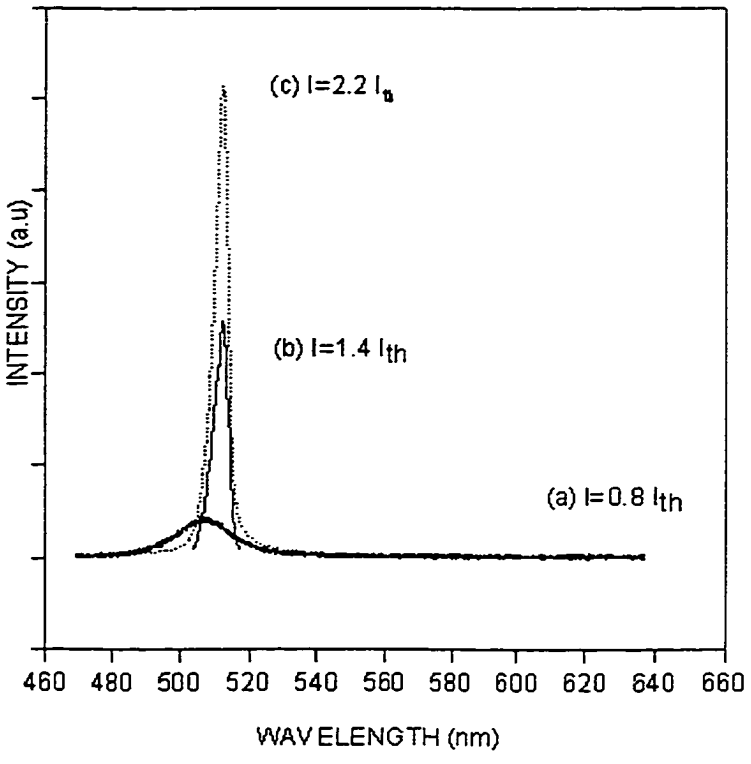

Figure 3.10 Spectra of edge emission from a laser sample below the threshold pumping intensity (a) and above the lasing threshold (b and c).

The temperature dependency of the threshold is an important characteristic relevant to the application of semiconductor lasers. The threshold of a semiconductor laser generally increases with increasing temperature. This is due to the reason that more carriers occupy the higher electronic states in the energy band at higher temperature, resulting in a lower carrier population at the states near the bandgap where the lasing action takes place. Thus higher pumping energy is needed for laser action at elevated temperatures. The temperature dependency of the threshold can be expressed by an empirical formula:

$$I = I_o \exp(\frac{T - T_1}{T_0}) \qquad (3.2)$$

Where I_0 is the threshold at an arbitrary reference temperature T_1, T is the absolute temperature, T_0 is the characteristic temperature often used to express the temperature sensitivity of threshold. Previous studies for III-V AlGaAs lasers and InGaAsP lasers show that the value of T_0 is affected by the carrier recombination mechanism [74][75] and carrier confinement [76][77]. In quantum-well lasers, the height of the energy barrier can affect the T_0 value. A lower energy barrier can result in smaller values of T_0 due to higher rate of carrier leakage out of the quantum-well with increasing temperature. We have measured the threshold density of a laser sample at three temperatures 2 C, 30 C and 47 C. (Figure 3.11). The threshold value

increases by 35% as the temperature is raised from 2 C to 47 C. From the temperature dependency of the threshold power density, the T_0 value is 150 K, which is comparable to those measured in GaAs/AlGaAs lasers.

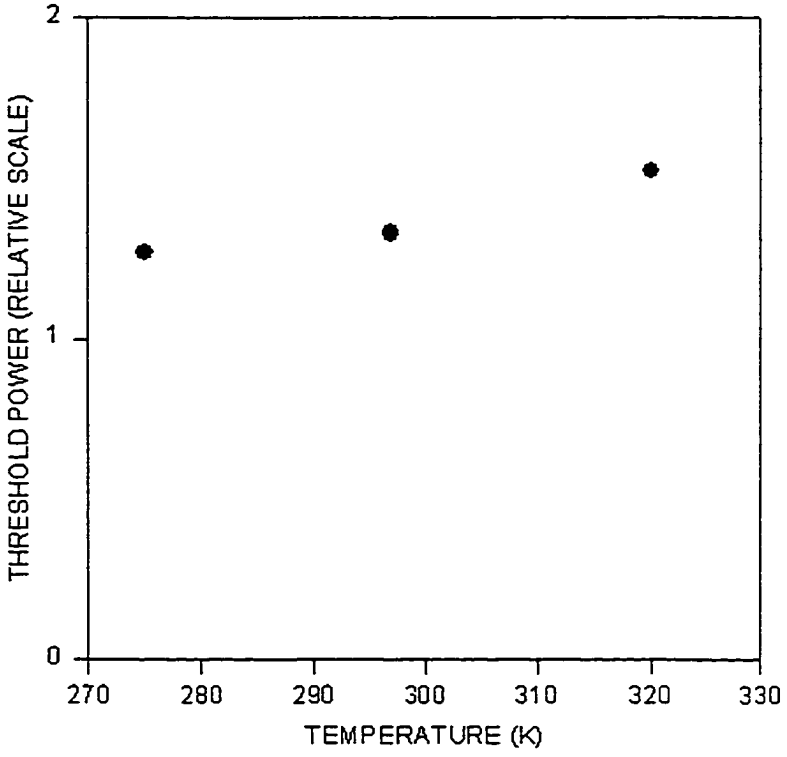

Figure 3.11 Pump power threshold varies as temperature changes

3.5 R-G-B optically pumped lasers

The bandgap energy of the quaternary material ZnCdMgSe depends on the compositions of Cd and Mg, as it is shown in Figure 3.2. In growing lattice matched and pseudomorphic laser samples, the bandgap energy of ZnCdMgSe waveguiding layer and cladding layer is around 2.7 eV and 3.0 eV respectively. The bandgap energy of the quantum well layer ZnCdSe is about 2.1 eV. The lasing wavelength is determined by the thickness and the composition of the quantum well layer[78].

Table 3.2 shows the parameters for three laser samples. Samples A and B are lattice-matched to the substrate InP. Sample C has excess cadmium in the quantum well layer, which causes 1.2% lattice mismatch to the substrate and results in compressive strain. The spontaneous emission wavelength of the quantum well was obtained from the 77 K photoluminescence spectrum.

Table 3.2 Parameters of three laser samples

Sample	QW thickness (nm)	QW mismatch (%)	QW emission wavelength at 77 K	QW lasing wavelength at room temperature (nm)
A	2.8	0	473	497
B	4.0	0	516	541
C	12.0	1.2	590	604

The lasing spectra of these samples are shown in figure 3.12. The stimulated emission peaks have a typical linewidth of about 5 nm, which is about a factor of 5 less than the linewidth of the spontaneous emission. The laser wavelength runs from blue (497 nm) to red (604 nm).

Since the parameters for this new material system, such as the effective masses, band offsets, and refractive indices, are not well characterized, no attempt has been made to optimize the device performance at the time of this study.

However it is shown that the crystalline quality of the II-VI materials can be improved dramatically by using Zn-irradiation and incorporating the initial low-temperature growth of ZnCdSe buffer layer on the InP substrate prior to quaternary material growth.[79] This addition is likely to reduce the interface roughness between the layers, also contributing to improved laser properties.

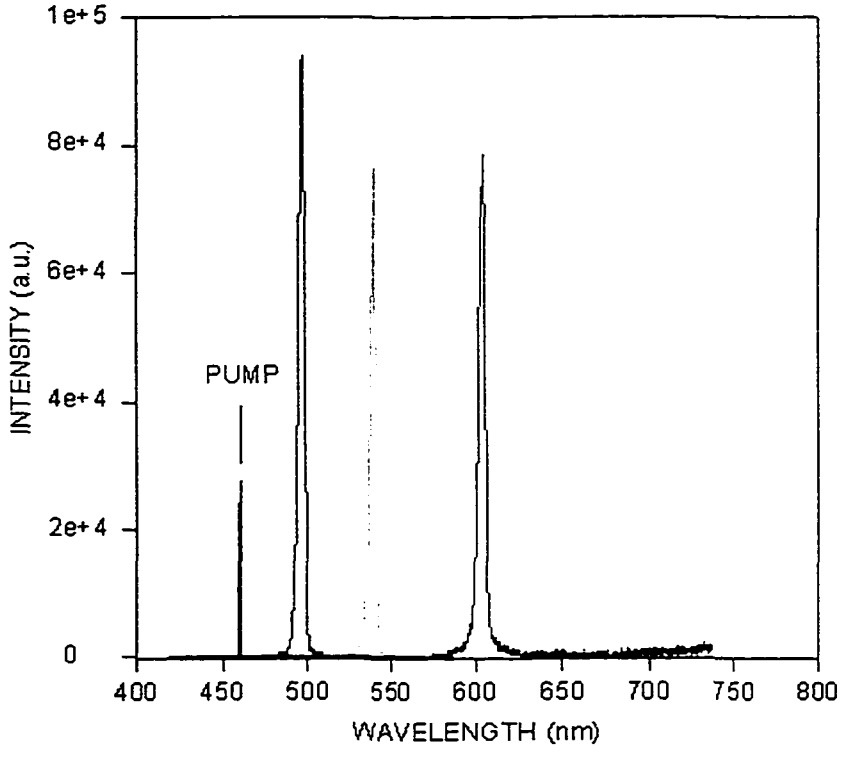

Figure 3.12 Lasing spectra of three ZnCdSe/ZnCdMgSe quantum-well lasers, whose parameters are listed in Table 3.2

Chapter 4 ZnCdSe/ZnCdMgSe light emitting diode

The photopumping experiment shows that ZnCdSe/ZnCdMgSe is a promising candidate for fabricating light emitting devices in the visible spectra range from red to blue. In this chapter, we will present the preliminary results of the operation of ZnCdSe/ZnCdMgSe light-emitting diodes.

4.1 p-n junction

With the introduction of chloride for n-type doping and activated nitrogen for p-type doping to the MBE growth chamber, the dopant density can reach a level higher than 10^{20} cm^{-3} in n-ZnSe and p-ZnTe. By using a p-ZnSeTe layer or p-ZnSe/ZnTe superlattice, the Ohmic contact can be easily achieved. Thus it is now possible to fabricate ZnCdSe/ZnCdMgSe laser diode (LD) or light emitting diode (LED).

The light-emitting diode used in this study has a quantum-well structure similar to that of a photopumped laser diode. Figure 4.1 shows its layer structure. All layers except the quantum well layer for red emission were grown lattice-matched or to the InP substrate.

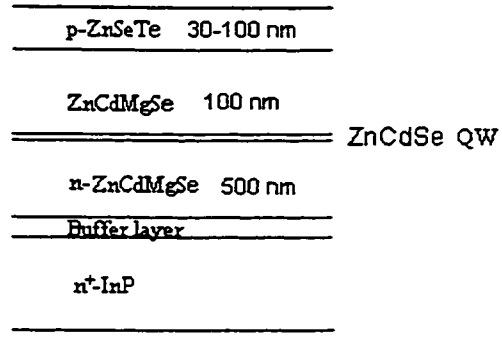

Figure 4.1. Schematic structure of a ZnCdSe/ZnCdMgSe light-emitting diode

The quaternary material ZnCdMgSe can be doped n-type to about 10^{18} cm^{-3} by using $ZnCl_2$. But the p-type doping of ZnCdMgSe is difficult to achieve. To make p-contact layer, another material, which can be easily p-doped, has to be grown on top of the ZnCdMgSe layer. In our study, lattice-matched ZnSeTe is used for the p-contact layer, because it can be easily p-doped to a high level to facilitate an Ohmic contact with gold. Another advantage of growing a ZnSeTe contact layer is that it can be grown lattice matched to the substrate InP, and thus produces low defect density. Faschinger et al[80] showed that the ZnSeTe material could be easily p-type doped even with a small content of tellurium. The hole concentration increases significantly with the increase of the content of tellurium until a saturation is reached at a hole concentration of 10^{20} cm^{-3} when the tellurium content is greater than 40%. It was also shown that an Ohmic contact can be formed by

evaporating a gold layer on the p-ZnSeTe contact layer even at low hole concentration of 2×10^{16} cm^{-3}.

In constructing the band alignment for the ZnCdSe/ZnCdMgSe heterostructure shown in Figure 4.1, the "common anion" and "common cation" rules provide a useful guide. The "common anion/cation"rules state that when two materials have same anion/cation, the bands are aligned at the valence/conduction band and the band discontinuity mostly appears in the conduction/valence band. But if two cations have different electronic structure, like Mg (d orbital unoccupied) and Zn (d orbital full), the "common anion" rule may not apply and a large valence band offset may occur.[81]

Figure 4.2 (a) shows the band lineup for binary materials ZnSe, ZnTe and CdSe.[82] The "Common anion/cation" rules apply well to these binary materials. Both ZnSe and ZnTe have a common anion Zn, so the conduction band discontinuity is small compare to the large valence band difference. Both ZnSe and CdSe have a common cation Se, thus the band aligns to the valence band and a large conduction band difference appears.

To construct the band lineup for ZnCdSe/ZnCdMgSe/ZnSeTe, we assume that ZnSe and ZnCdSe are lineup to the valence band, ZnSe and ZnSeTe are lineup to the conduction band, while ZnCdSe and ZnCdMgSe have large discontinuities in both the conduction band and valence band.

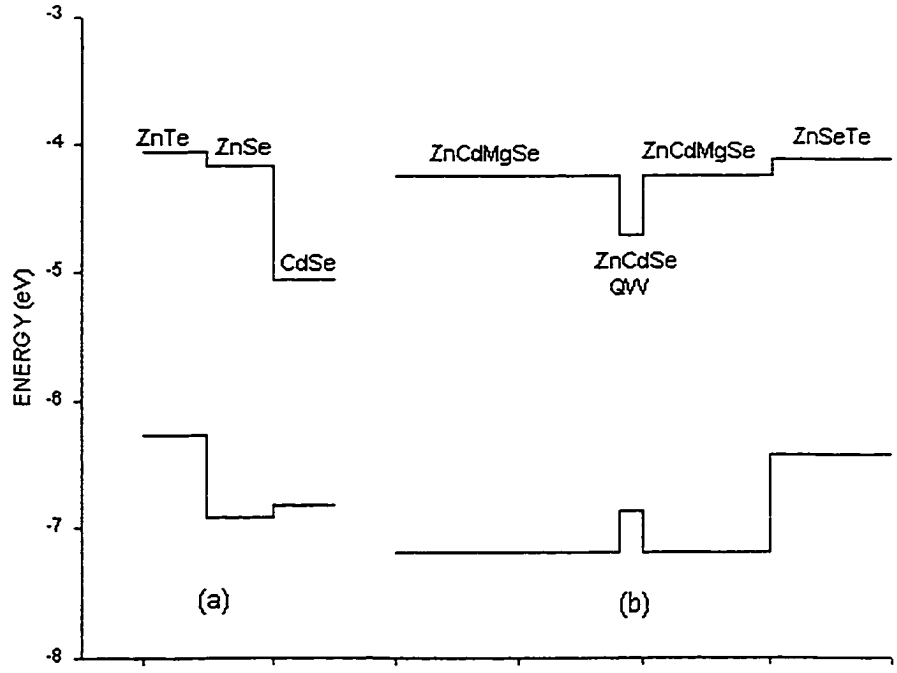

Figure 4.2. Schematic band lineup for ZnCdSe/ZnCdMgSe/ZnSeTe

The band lineup for ZnCdMgSe and ZnSeTe is not known. Iwata et al[83] showed a type-II band lineup with small discontinuity on the conduction band. But the position of the conduction band of ZnCdMgSe largely depends on the composition of Mg in the material, a type-I band lineup is

possible for a large Mg concentration. Figure 4.2 (b) shows the presumed band lineup for an undoped ZnCdMgSe/ZnCdSe/ZnCdMgSe/ZnSeTe light emitting diode structure based on the above discussion.

For the ZnCdSe/ZnCdMgSe heterostructure, the band lineup is always type-I at any Mg concentration.[83] From our photopumping experiment on the laser samples which are fabricated from the same material system, laser operation is realized up to temperature of about 350 K. Thus we can assume that the band offsets in both the conduction band and valence band are large enough to confine the carriers at room temperature.

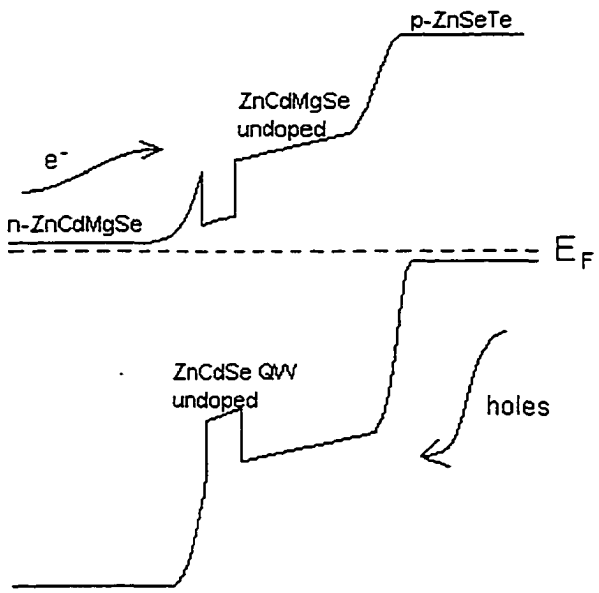

Figure 4.3. Schematic band profile of ZnCdSe/ZnCdMgSe/ZnSeTe hetero-structure under zero bias.

Doping of the material causes band bending at the interface. Figure 4.3. shows the assumed band profile of the ZnCdSe/ZnCdMgSe/ZnSeTe hetero-structure under zero bias. From the diagram, it is clear that there is a rather large potential barrier, estimated to be about 0.7 eV, at the p-ZnSeTe/ZnCdMgSe interface (on the p-side) for the holes to be injected into the quantum well layer. This barrier will certainly contribute to a higher turn-on voltage.

4.2 I-V characteristics of LED

The current-voltage characteristics for a diode is given by the Shockley equation

$$I=I_{s0}[\exp(eV_d/\gamma kT)-1] \qquad (4.1)$$

where I is the current flow through the diode, V_d is the potential drop across the diode, I_{s0} is the saturation current, k is the Boltzmann constant, T is the absolute temperature and γ is a constant between 1 and 2, where $\gamma=1$ for an ideal diode. The measured voltage V across a diode is

$$V=V_d+IR \qquad (4.2)$$

where R is the diode series resistance. The series resistance accounts for the contact resistance and the combined resistance of the layers.

Equation (4.1) now becomes

$$I=I_{s0}\{\exp[(eV-eV_d)/\gamma kT]-1\} \quad (4.3)$$

Equation (4.3) describes the I-V characteristic for a realistic diode.

Figures 4.4-4.5 show the I-V characteristics of two ZnCdSe/ZnCdMgSe light emitting diodes with an indium contact. The data are provided by professor Tamargo's group at City College, but our pulsed I-V measurement also exhibits similar feature. The turn-on voltage is around 5V, which is larger than the bandgap energy of the ZnCdSe quantum-welllayer (about 2.1 eV). The large turn-on voltage is attributed to the large potential barrier at the ZnCdMgSe/ZnSeTe interface as illustrated in Figure 4.3. The typical value of the serial resistance of the LED, derived from the slope of the linear portion of the I-V characteristic, is about 13 Ohm. Based on the 0.25 mm-diameter contact area, the resistivity–thickness product (ρL) of the device is 2.5×10^{-2} Ohm•cm^2, where the resistivity is believed to be caused mainly by the p-side layers. In comparison, the corresponding ρL value for the state-of-the art GaAs laser is 4.2×10^{-4} Ohm•cm^2, which is two orders of magnitude smaller. Thus improving the conductivity of the p-layer and the quality of the p–contact remain a major challenge.

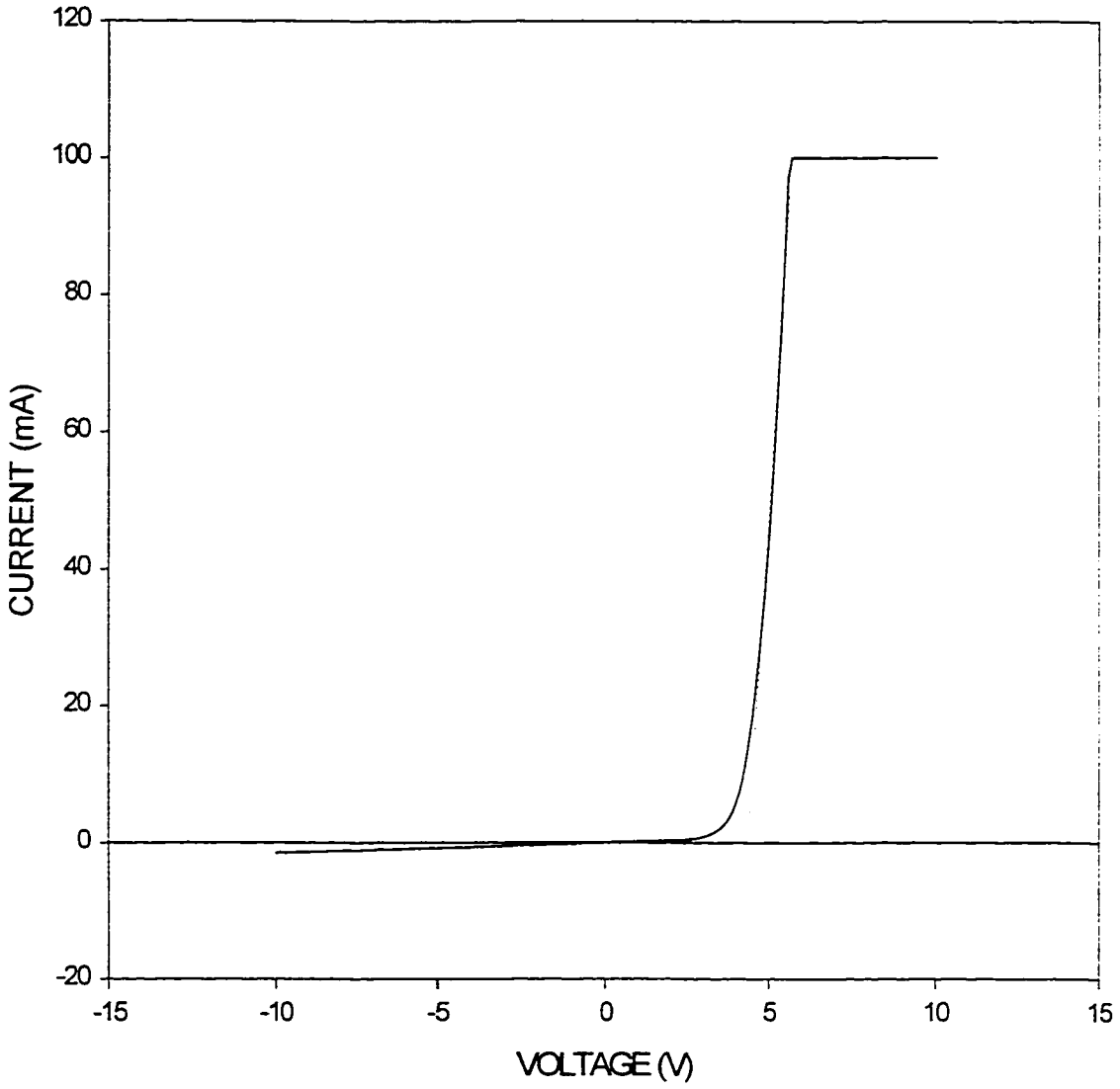

Figure 4.4 I-V characteristic for Sample 1013 with indium contact. The resistance of the diode determined from the slope of the linear portion is R=13 Ohm.

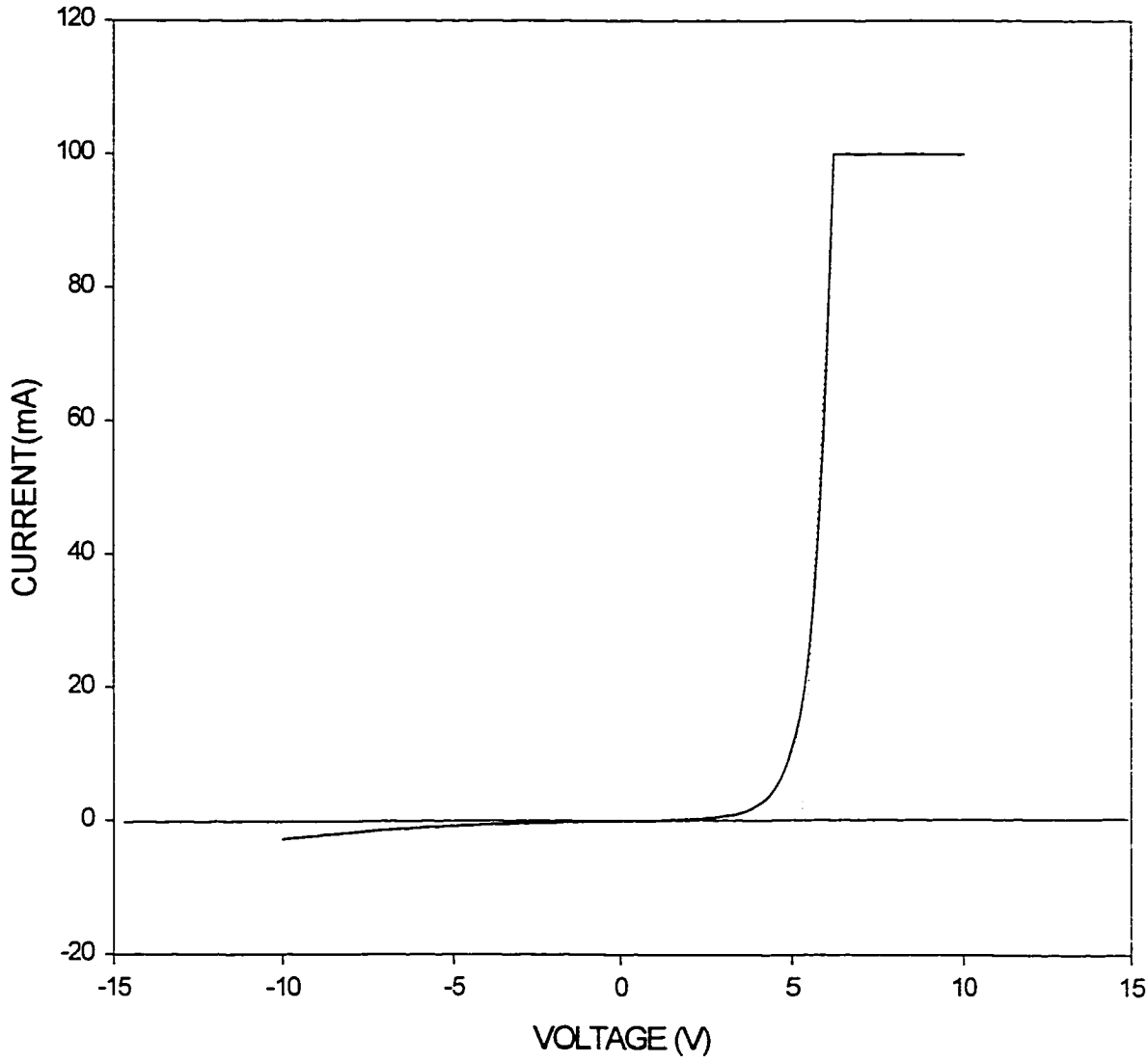

Figure 4.5 I-V curve for Sample 1083. The resistance of the diode determined from the slope of the linear portion is R=14 Ohm.

4.3 Electro-luminescence of the LEDs

Since the diodes tended to degrade under CW operation, the electro-luminescence measurement was done using a pulse generator to drive the light emitting diode. The experimental setup is shown in Figure 4.6. The current pulses were about 600-ns long. The repetition rate was 8 kHz. The current through the LED was monitored using a magnetic current probe and the waveform was displayed on a digital oscilloscope.

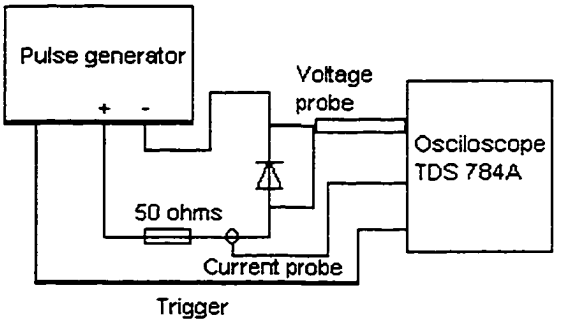

Figure 4.6 The electronics used to drive the diode and to monitor the current through the diode.

The emission of the LED samples was collected using a microscope objective and analyzed using a monochromatic spectrometer, which has a CCD camera attached to the exit port. The room temperature electro-luminescence spectra are shown in Figures 4.7-4.9.

The layer structure of the LED is shown in Figure 4.1. The parameters of the three LEDs used in the experiment are listed in Table 5.1. All layers of the Samples 1013 and 1083 are lattice-matched to the InP substrate. The quantum-well layer in Sample 1088 is pseudomorphic with a lattice mismatch of 1.2%.

Table 5.1 Parameters of LED Samples 1013, 1083 and 1088

Sample	Thickness and bandgap energy				Lattice mismatch in the QW layer
	ZnSeTe cap	p-ZnCdMgSe	n-ZnCdMgSe	ZnCdSe QW	
1013	100 nm	100 nm	500 nm	6 nm	0
	E_g=2.2 eV	E_g=2.85 eV*	E_g=2.85 eV*	E_g=2.32 eV*	
1083	30 nm	100 nm	500 nm	2 nm	0
	E_g=2.2 eV	E_g=2.85 eV*	E_g=2.85 eV*	E_g=2.5 eV*	
1088	50 nm	100 nm	500 nm	10 nm	1.2%
	E_g=2.2 eV	E_g=2.53 eV*	E_g=2.53 eV*	E_g=2.02eV*	

* E_g is the bandgap energy estimated from photoluminescence measurement at 77 K.

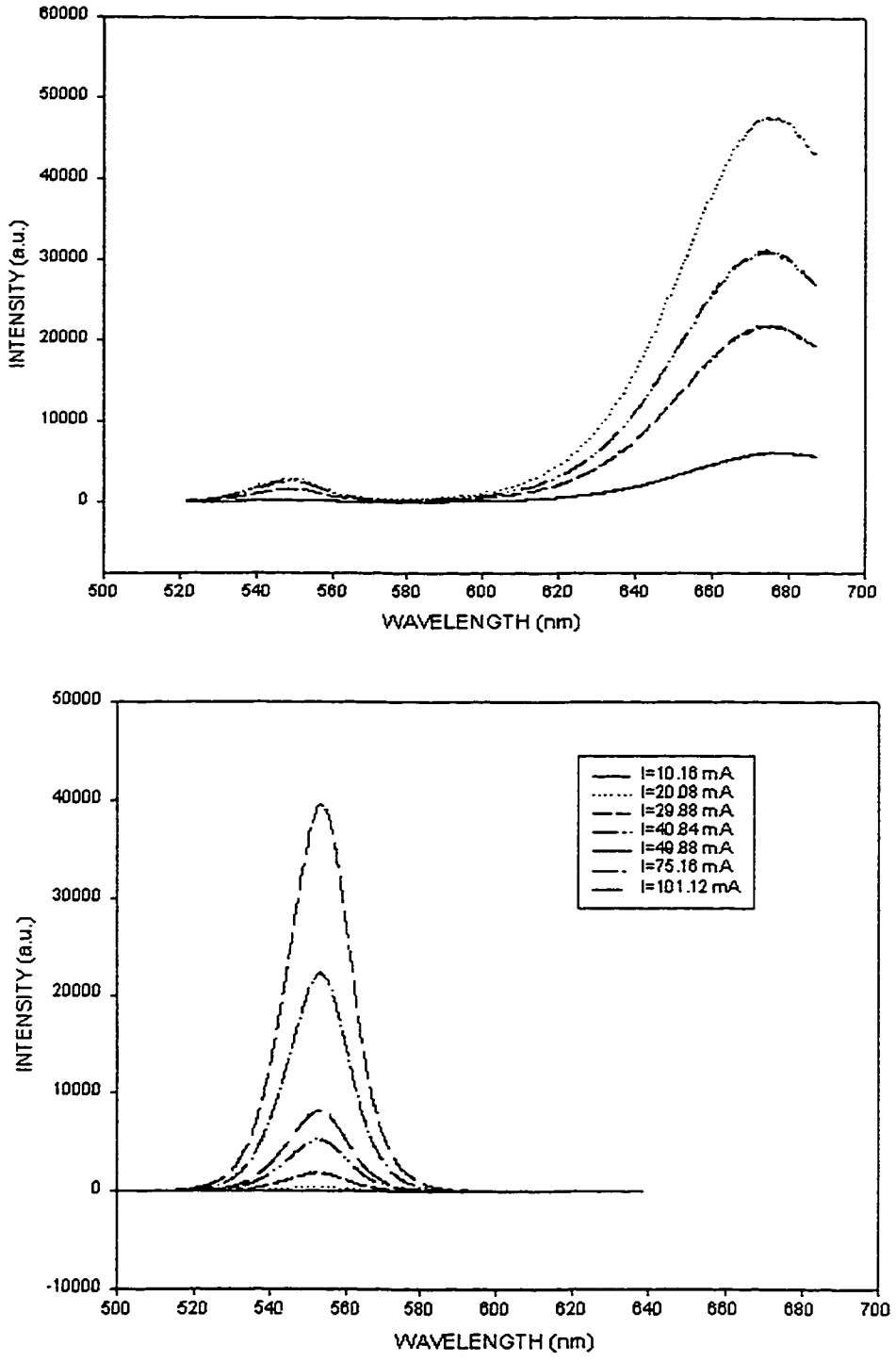

Figure 4.7 Spectra for Sample 1013. The upper graph shows the spectra for the as-grown sample. The peaks at 550 nm and 670 nm are attributed to the quantum well and the ZnSeTe layer respectively. The lower graph is the spectra when most of the ZnSeTe top layer was removed. Only the emission at 550 nm from the quantum well is present.

Figure 4.7 shows the electro-luminescence spectra of Sample 1013 at different pump currents. The upper graph shows the spectra for the as-grown sample. The peak at 550 nm is attributed to the emission of the quantum well according to the design. In addition to the quantum well emission, a much stronger emission at 670 nm was also observed. The lower graph shows the spectra for the same sample after most of the top ZnSeTe layer was removed. The emission from the quantum well at 550 nm was unchanged, but the peak at 670 nm disappeared. There is no apparent peak shift for the quantum well emission taken at different pump current level, indicating that the carrier densities are quite low.

The low temperature PL of Sample 1013, shown in Figure 4.8, displayed a similar broad red tail on the longer wavelength side of the spectrum. The emission from the quantum well was at about 536 nm. The emission at about 433 nm is attributed to the ZnCdMgSe cladding layer. The broad emission beyond 600 nm is attributed to the ZnSeTe cap layer. The tellurium is known to form deep traps in ZnSe, which are responsible for very broad and intense photoluminescence emission.[84] Thus the emission at

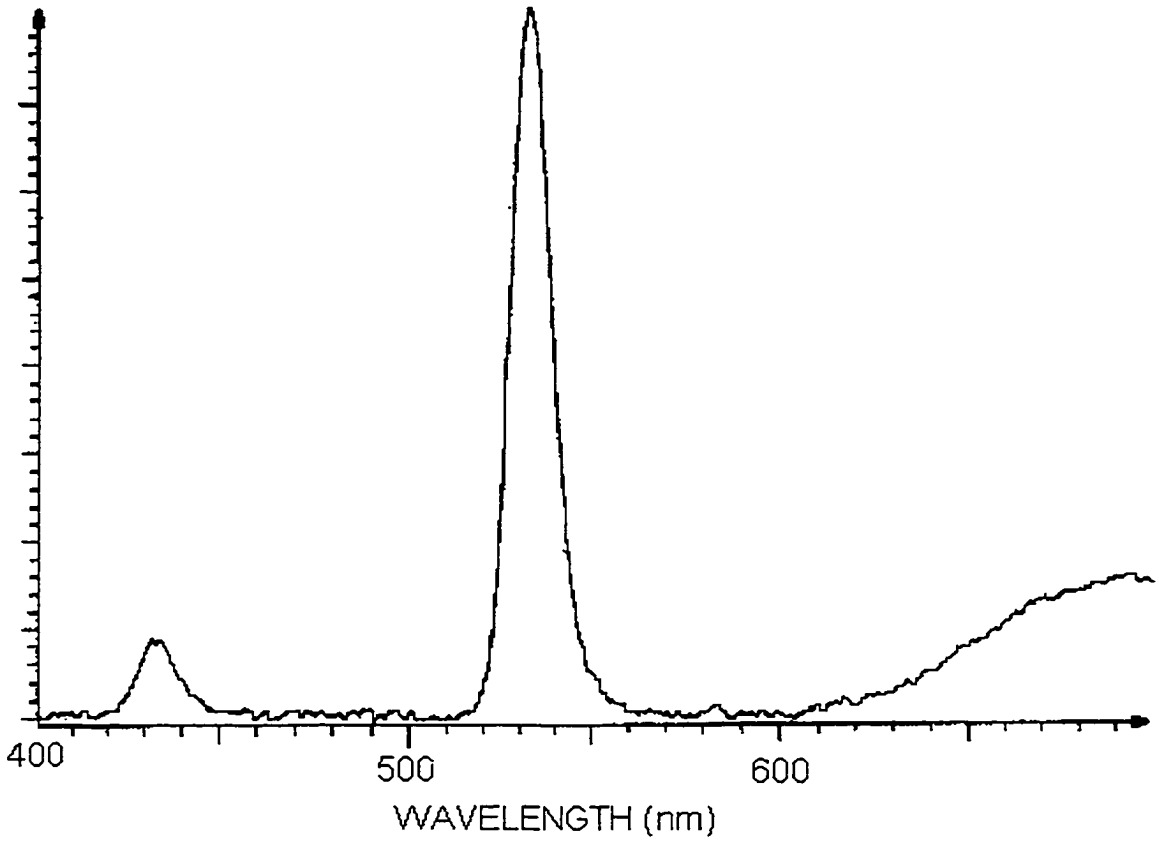

Figure 4.8 Low temperature (77 K) photoluminescence spectrum of Sample 1013. The peaks at 433 nm, 536 nm and 690 nm are attributed to the ZnCdMgSe cladding layer, ZnCdSe quantum well layer and the top ZnSeTe layer respectively.

660 nm is believed to be the photoluminescence of the ZnSeTe after absorbing the electro-luminescence at 550 nm.

Figure 4.9 shows the spectra for Sample LED 1088 emitting in the red. Here again we see the broad tails on the longer wavelength side of the spectrum, which is attributed to the top ZnSeTe layer. The sample's top layer is partially etched, so the emission in the red is weaker than that of the Sample 1013. At smaller pump currents, the contribution from the top layer is more pronounced. The inset in Figure 4.9 shows the spectrum taken at1.00 mA. The ratio of the peak intensities from the QW and that from the ZnSeTe layer is about 3:1. As the pump current increases, the contribution from the QW increases rapidly. The ratio of the peak intensities becomes 16:1 at a pump current of I=100 mA. The increase of the ratio indicates that the absorption from the ZnSeTe layer is saturated. The peak emission wavelength from the quantum well is at 630 nm at all the pump currents.

The emission wavelength of the ZnCdSe/ZnCdMgSe quantum-well LEDs depends on the width of the quantum well. This feature has been

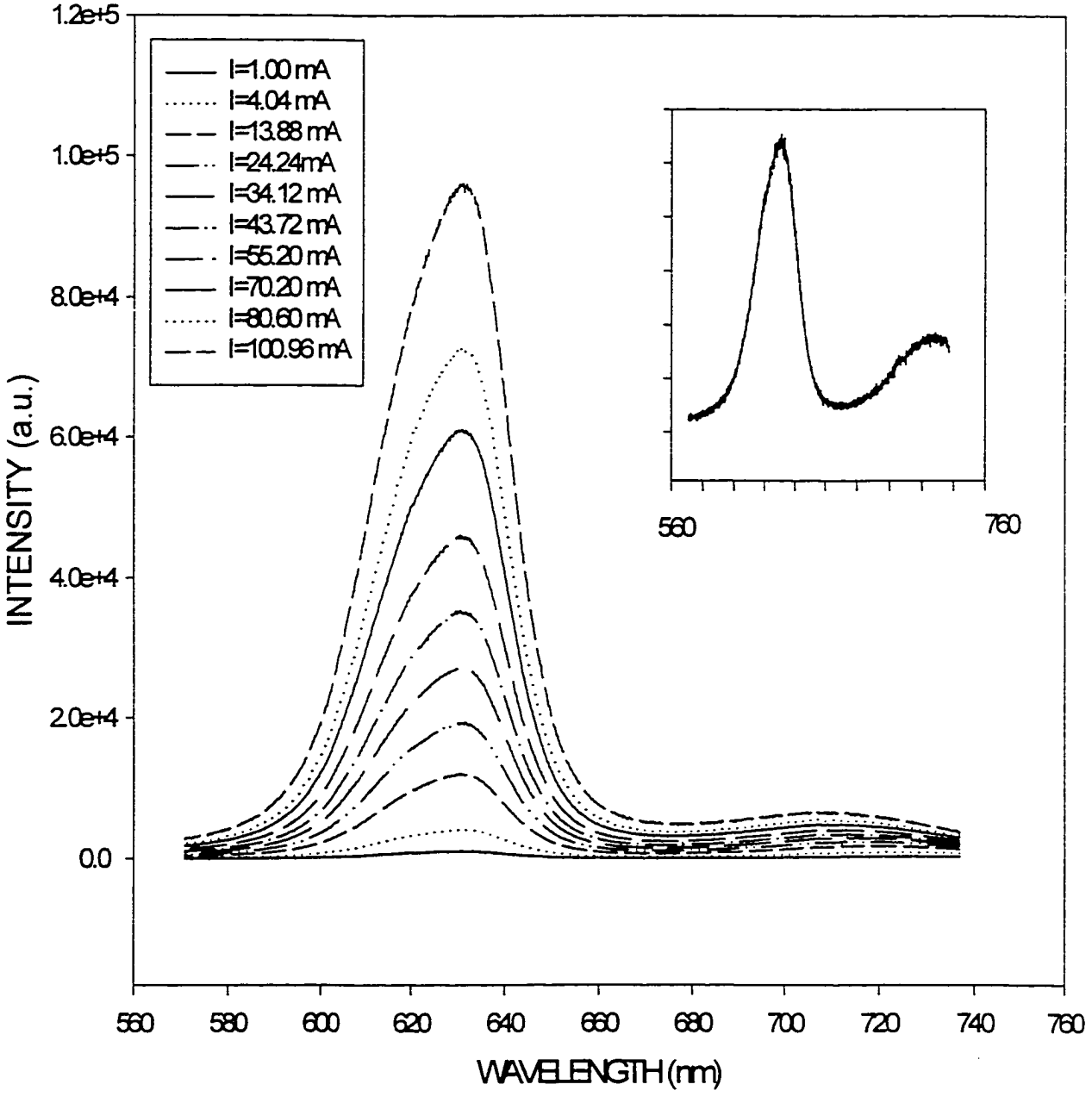

Figure 4.9 Spectra from a red LED. The inset shows the spectrum taken at 1 mA. The ratio of the two peak intensities is about 3:1. At 100 mA, that ratio becomes 16:1.

demonstrated in photopumped lasers described in Chapter 3. Figure 4.10 shows the spectra for three LEDs. The emission wavelength are 520 nm, 550 nm and 630 nm for Samples 1083, 1013 and 1088 respectively. The emission intensities of the blue/green LEDs are much weaker than that of the red LED. This is consistent with our understanding that the top ZnSeTe layer whose bandgap is about 2.2 eV absorbs the emission from the quantum well, resulting in much weaker blue and green LED emission. It is also consistent with the fact that the blue/green LED has a much thinner quantum well layer.

Figure 4.11 shows the dependence of the power emission from LED as a function of pump current from Samples 1013 and 1088. At smaller pump current, the output power vs current is super-linear. At larger pump current, the output power is linearly proportional to the pump current. The linear dependence of output light power on input current suggests that each carrier injected to the quantum well is assumed to lead, via recombination with a hole, to the emission of a photon. In this range of the injection current, the effects of the current leakage due to the finite potential height of the quantum well and thermal motion of the carriers and carrier recombination process with defects are insignificant.

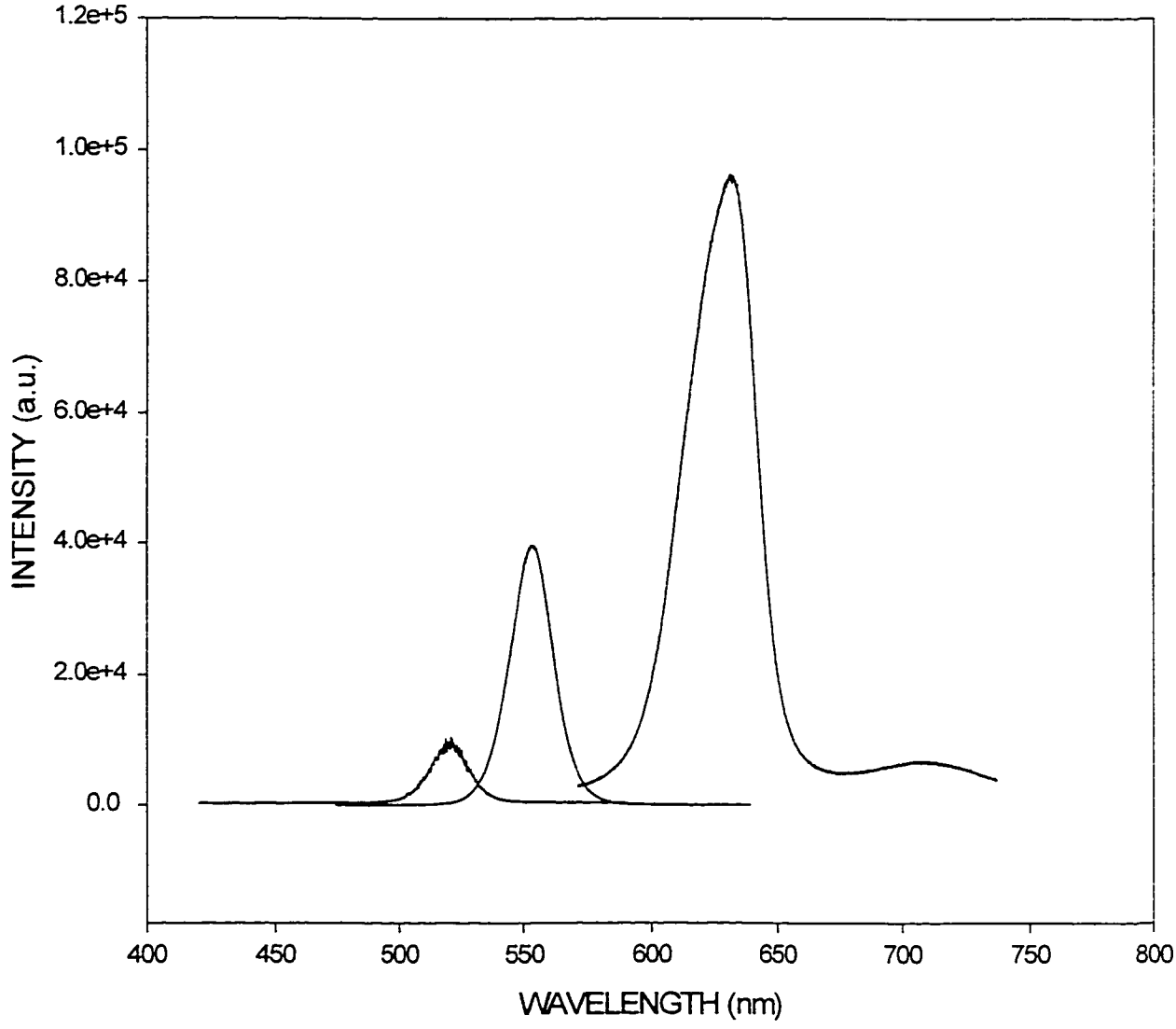

Figure 4.10 Spectra for three LEDs. The widths of the quantum wells for Samples 1083, 1013 and 10 88 are 2 nm, 6 nm and 10 nm respectively.

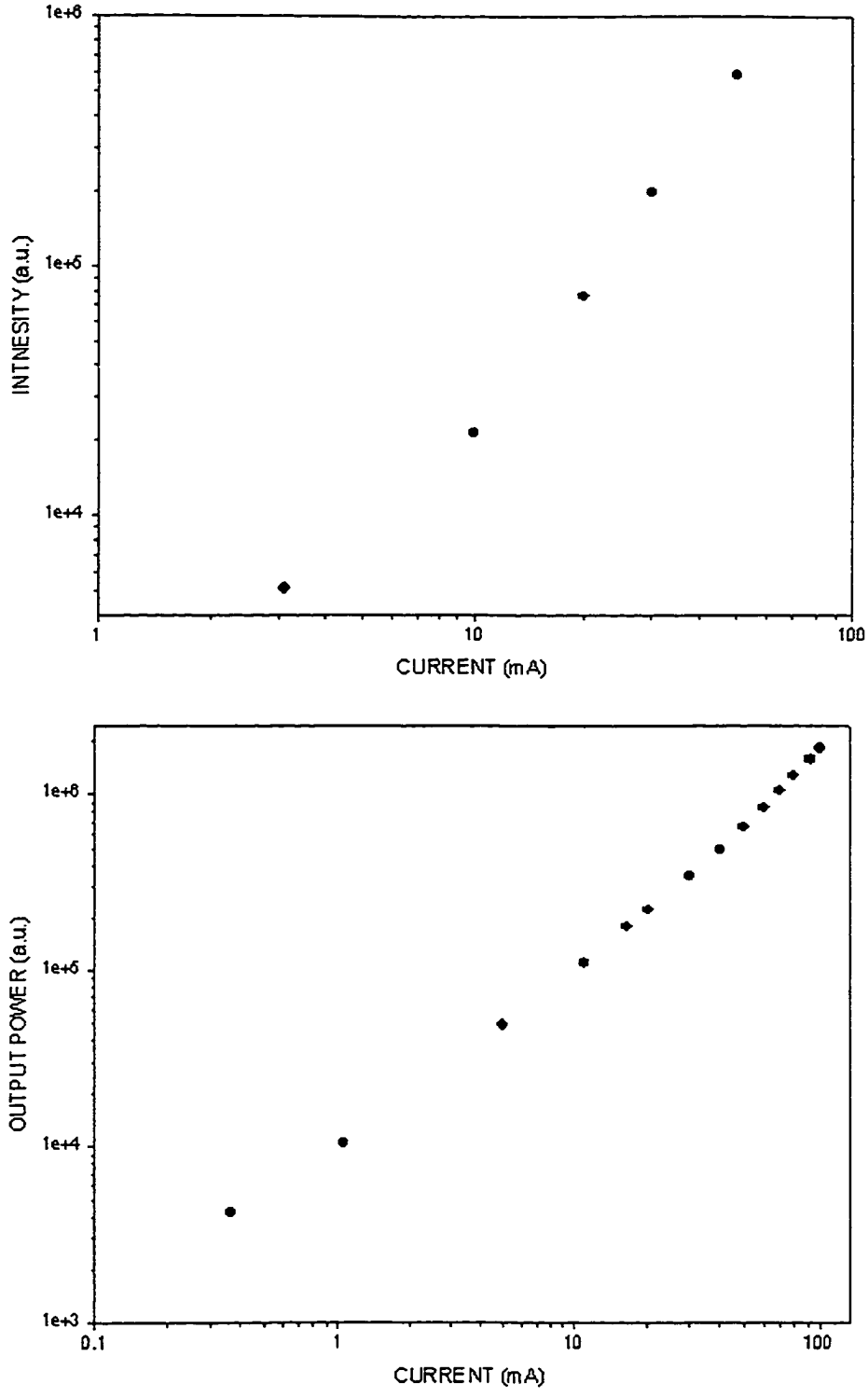

Figure 4.11 Output light power as a function of pump current. The upper graph shows the light intensity dependency on pump current for a green LED (Sample 1013). The lower graph is for a red LED (Sample 1088). At larger pump current, the dependency of the output light power on the pump current is nearly linear.

Chapter 5 Study of gain profile for ZnCdSe/ZnCdMgSe quantum-well laser

5.1 Introduction

The gain profile of a gain medium can be deduced from the spectrum of the spontaneous emission based on the theory proposed by Henry et al[85].

Consider a beam with n photons per optical mode passing through a thin layer of semiconductor with path length x. The change of the photon number can be expressed as:

$$\Delta n = -\alpha x n + A + Bn \qquad (5.1)$$

where α is absorption coefficient, n is the photon number, A is the spontaneous emission coefficient and B is the stimulated emission coefficient.

The first term in the right side of the Equation 5.1 is the number of photons being absorbed. The second and the third terms are photons generated from spontaneous emission and stimulated emission, respectively.

It can be shown that the coefficient for spontaneous emission in a

semiconductor medium with a quasi-Fermi level separation eV and photon energy $h\nu$ is

$$A = \alpha x \exp(\frac{eV - h\upsilon}{kT}) \tag{5.2}$$

where h is Plank constant, ν is the frequency of light, k is Boltzmann constant and T is the absolute temperature.

The rate of spontaneous emission entering a single mode is given by

$$\frac{dA}{dt} = \frac{dx}{dt} \bullet \frac{dA}{dx} = \frac{c}{\mu}\frac{dA}{dx} = \alpha \frac{c}{\mu}\exp(\frac{eV - h\nu}{kT}) \tag{5.3}$$

where c is the speed of light, μ is the refractive index of the semiconductor. The number of modes per unit solid angle per unit frequency and per unit volume is

$$\frac{dN}{Vd\nu d\Omega} = \frac{8\pi\mu^3(h\nu)^2}{h^2c^3} \tag{5.4}$$

where V is the volume, $d\nu$ is the frequency interval and $d\Omega$ is the solid angle.

The spontaneous emission intensity $I(h\nu,eV)$ at photon energy $h\nu$ and quasi-Fermi level separation eV is proportional to the product of spontaneous

emission rate per mode and the number of modes, that is, the product of Equations (5.3) and (5.4), i.e.

$$I(h\nu,eV)=8\pi\mu^2(h\nu)^2\alpha(h\nu,eV)\exp[(eV-h\nu)/kT]/(h^2c^2) \quad (5.5)$$

The quasi-Fermi level separation eV can be determined from the spontaneous emission spectrum taken at two different pumping levels.

$$\frac{I(h\nu,eV)}{I(h\nu,eV_L)}=\frac{\alpha(h\nu,eV)}{\alpha(h\nu,eV_L)}\exp(\frac{eV-eV_L}{kT}) \quad (5.6)$$

where eV_L is the Fermi level separation at lasing threshold. For sufficiently high photon energy, the absorption coefficient α is independent of eV, then

$$\frac{I(h\nu,eV)}{I(h\nu,eV_L)}=\exp(\frac{eV-eV_L}{kT}) \quad (5.7)$$

Thus the ratio of the intensities of the spontaneous emission at different pumping levels will differ only by a factor of $\exp[(eV-eV_L)/kT]$. In the high-energy region where the photon energy is far above the absorption edge, the spectra are linear in the log scale.

For a given pumping level characterized by the quasi-Fermi level separation eV, the optical gain $g(h\nu,eV)$ is related to the absorption coefficient $\alpha(h\nu,eV)$ by the following formula:

$$g(h\nu,eV)=\alpha(h\nu,eV)\{\exp(\frac{eV-h\nu}{kT})-1\} \quad (5.8)$$

Combining Equation (5.8) with Equation (5.5), the gain spectrum at quasi-Fermi level separation eV is

$$g(h\nu,eV)=\frac{(hc)^2 I(h\nu,eV)}{8\pi\mu^2(h\nu)^2}\bullet\{1-\exp(\frac{h\nu-eV}{kT})\} \quad (5.9)$$

Equations (5.7) and (5.9) can be used to deduce the gain profile from the spontaneous spectrum.

5.2 Spontaneous emission spectrum

The sample used to study the gain profile is Sample 471 with a step index profile, whose layer structure consists of a 10-nm-thick active layer buried in 120-nm-thick waveguiding layers and 440-nm-thick cladding layers. The low temperature spectrum shows the bandgap energy of 2.10 eV, 2.90 eV and 3.13 eV for the active layer, waveguiding layers, and cladding layers, respectively. The lasing spectrum of this sample is shown in Figure 5.1.

The experimental setup for the measurement of the spontaneous emission spectrum is shown in Figure 5.2. The surface emission of the sample was collected with a microscopic objective and focused on the entrance slit of the

monochromatic spectrometer. A series of spectra, shown in Figure 5.3, were taken at different pumping levels. When the pump intensity reached the laser threshold, a sharp spike appears at the lasing wavelength. The top most spectrum in Figure 5.3 was taken at a pump level just above the lasing threshold. The second spectrum was taken at threshold. The rest were taken at various pump intensities below threshold. The peaks of the spontaneous emission spectra shift to shorter wavelength at higher pump intensities, which is a result of band filling.

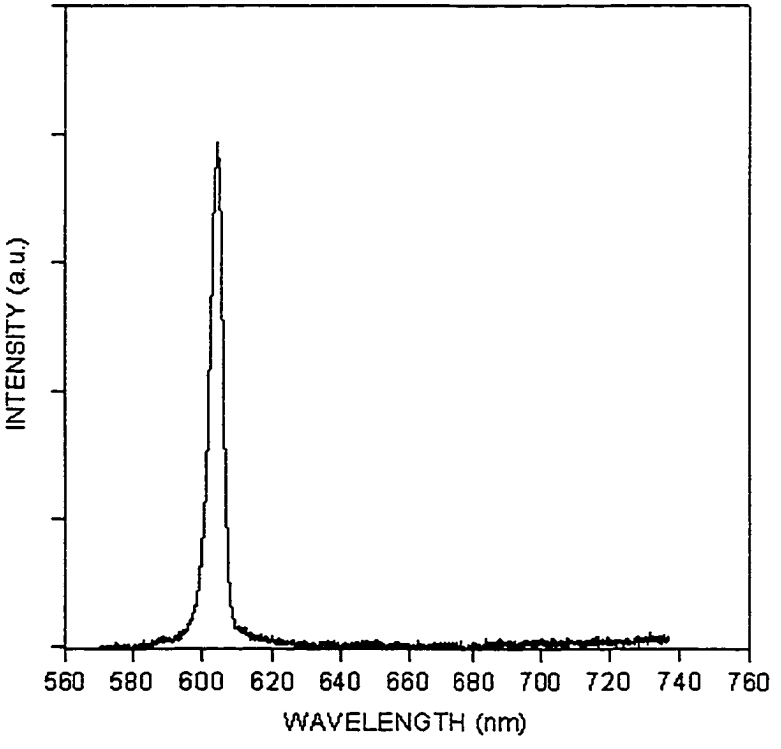

Figure 5.1 Lasing spectrum of Sample 471, when pumped by a dye laser.

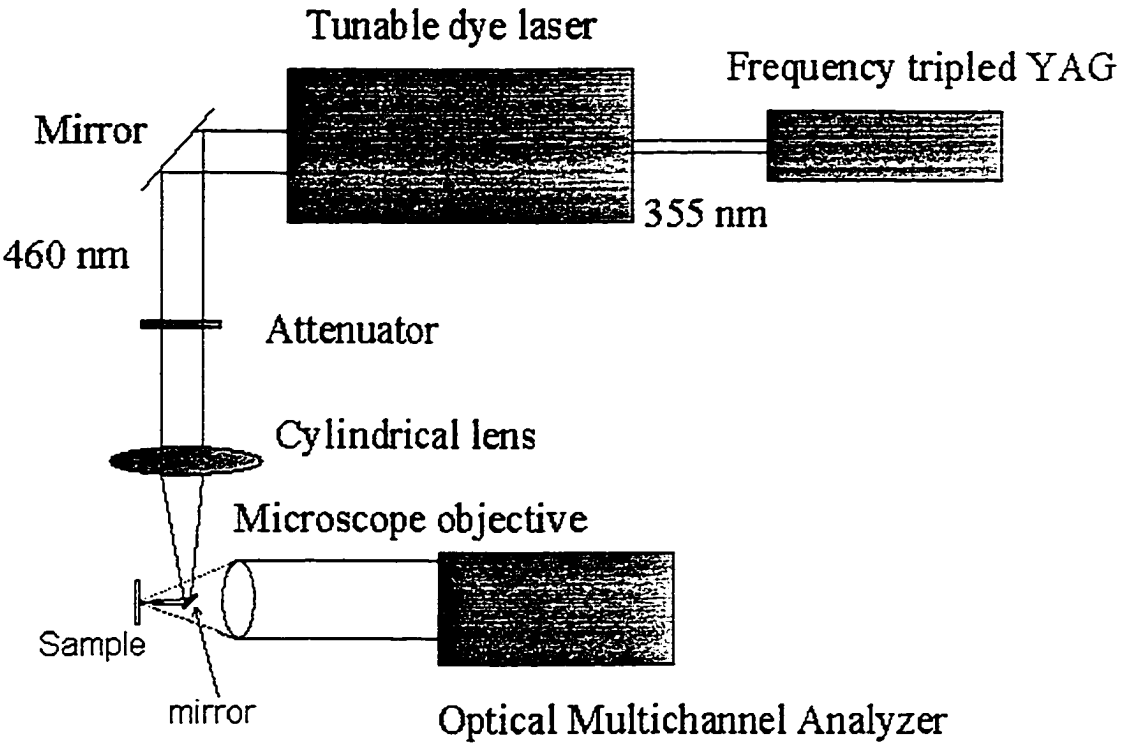

Figure 5.2 Experimental setup for spontaneous emission spectrum measurement

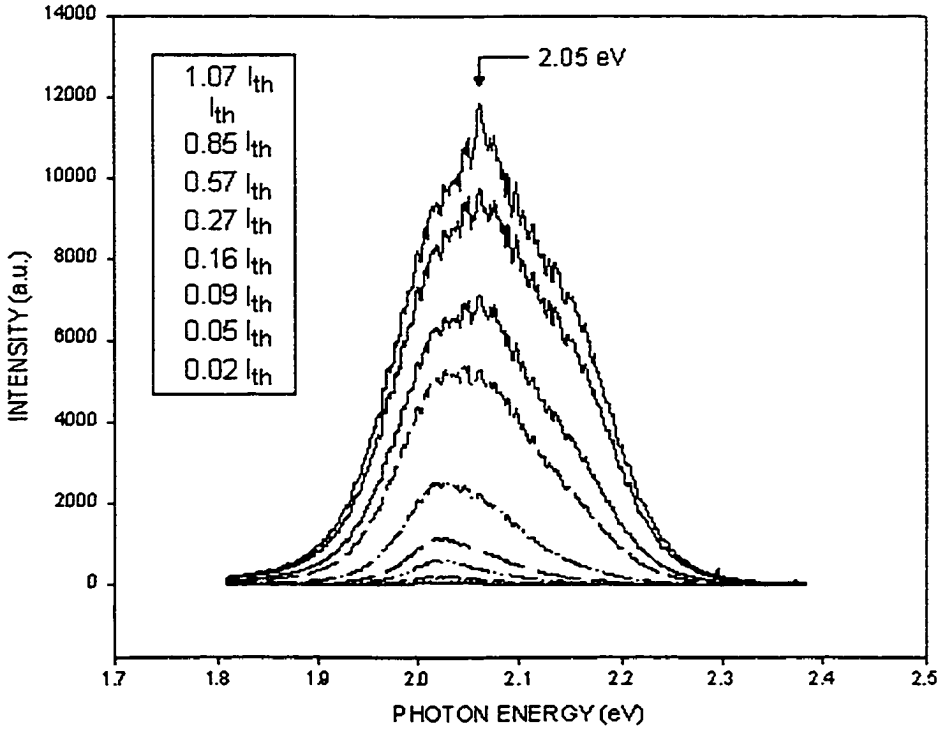

Figure 5.3 Spectra of spontaneous emission of Sample 471 taken at various pump intensities.

5.3 Optical gain profile

To deduce the gain profile, we need first to determined the quasi-Fermi level separation at lasing threshold. The gain coefficient at lasing threshold has a maximum at the lasing wavelength $h\nu=h\nu_L$. Where ν_L is the frequency of the laser, which, in our experiment, is the frequency of the sharp spike at 2.05 eV.

To determine eV_L, we apply Equation (5.9) to the emission spectrum taken at lasing threshold by assuming an arbitrary value of eV to generate a "trial" gain profile corresponding to the assumed value of eV. Changing the value of eV will change the shape of gain profile as well as the position of the maximum of the gain profile. If the maximum of the "trial" gain profile occurs at a frequency larger than the lasing frequency, we decrease the value of eV and apply Equation (5.9) again to get a new trial gain profile. If the maximum of the "trial" gain profile occurs at a frequency smaller than the lasing frequency, we increase the value of eV. This procedure is repeated until the maximum of the gain profile occurs at the lasing wavelength. The value of eV corresponding to this gain profile is eV_L.

Figure 5.4 shows the spontaneous spectra plotted in semi-log scale. Notice that at higher photon energy, the luminescence intensity as a function of photon energy exhibits a straight line, reflectingthe $\exp[(eV\text{-}eV_L)/kT]$ factor in Equation 5.7. This fact together with the knowledgeof eV_L can be used to determine the quasi-Fermi level separation by using Equation (5.7). The result is shown in Figure 5.5. As the pump intensity approaches the threshold, the quasi-Fermi level separation approaches a constant level. This behavior is fully expected for a laser operating above the thresholdbecause the laser action consumes the carriers at the same rate as the pumping rate.

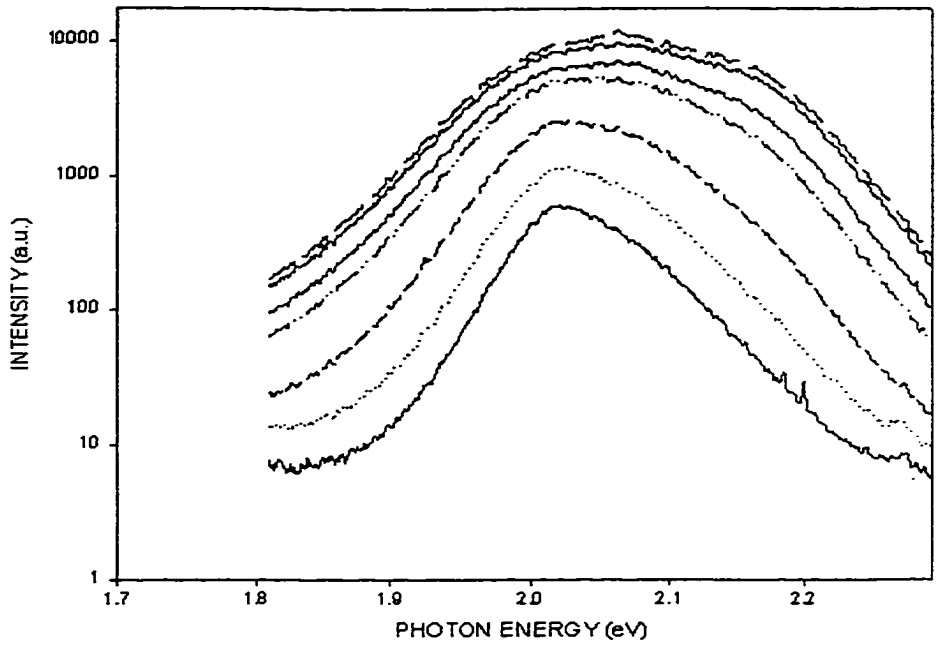

Figure 5.4 Emission spectra at different pump levels in semi-log scale. The top spectrum is taken at slightly above the threshold. The second top spectrum is taken at threshold. Other spectra are taken below the threshold.

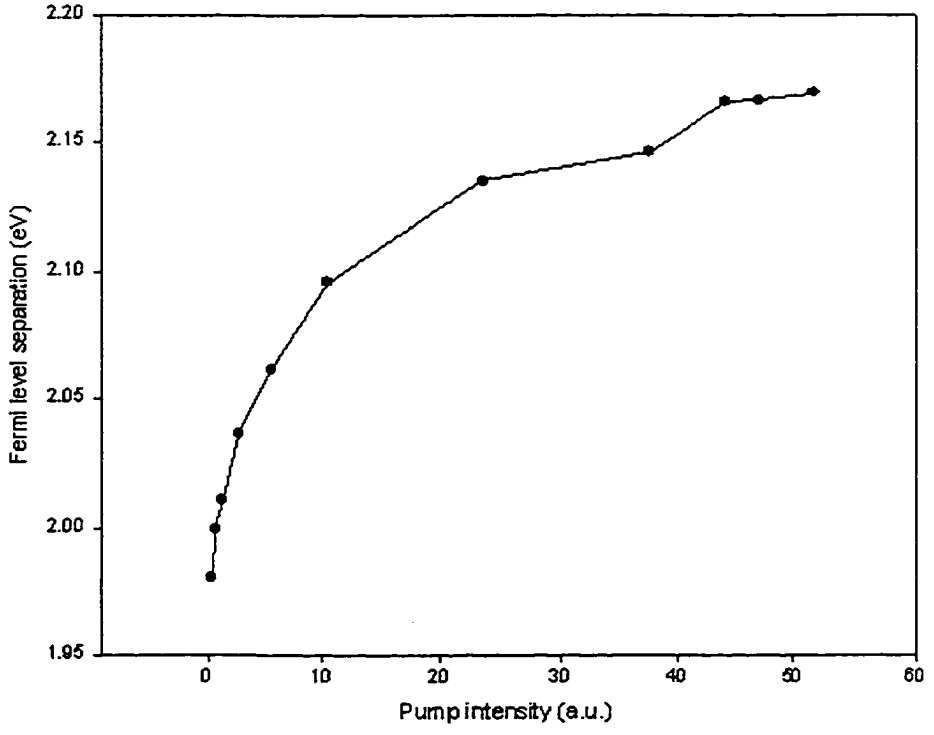

Figure 5.5 Quasi-Fermi level separation deduced from the spectra of Figure 5.4 as a function of pump intensity.

With the knowledge of quasi-Fermi level separation, the gain spectrum can be constructed from the spontaneous emission spectrum by using Equation (5.9). The result is shown in Figure 5.6.

The intercepts of the gain spectra at zero gain are the quasi-Fermi level separations. The full width at half maximum of the gain curve at threshold is about 0.15 eV.

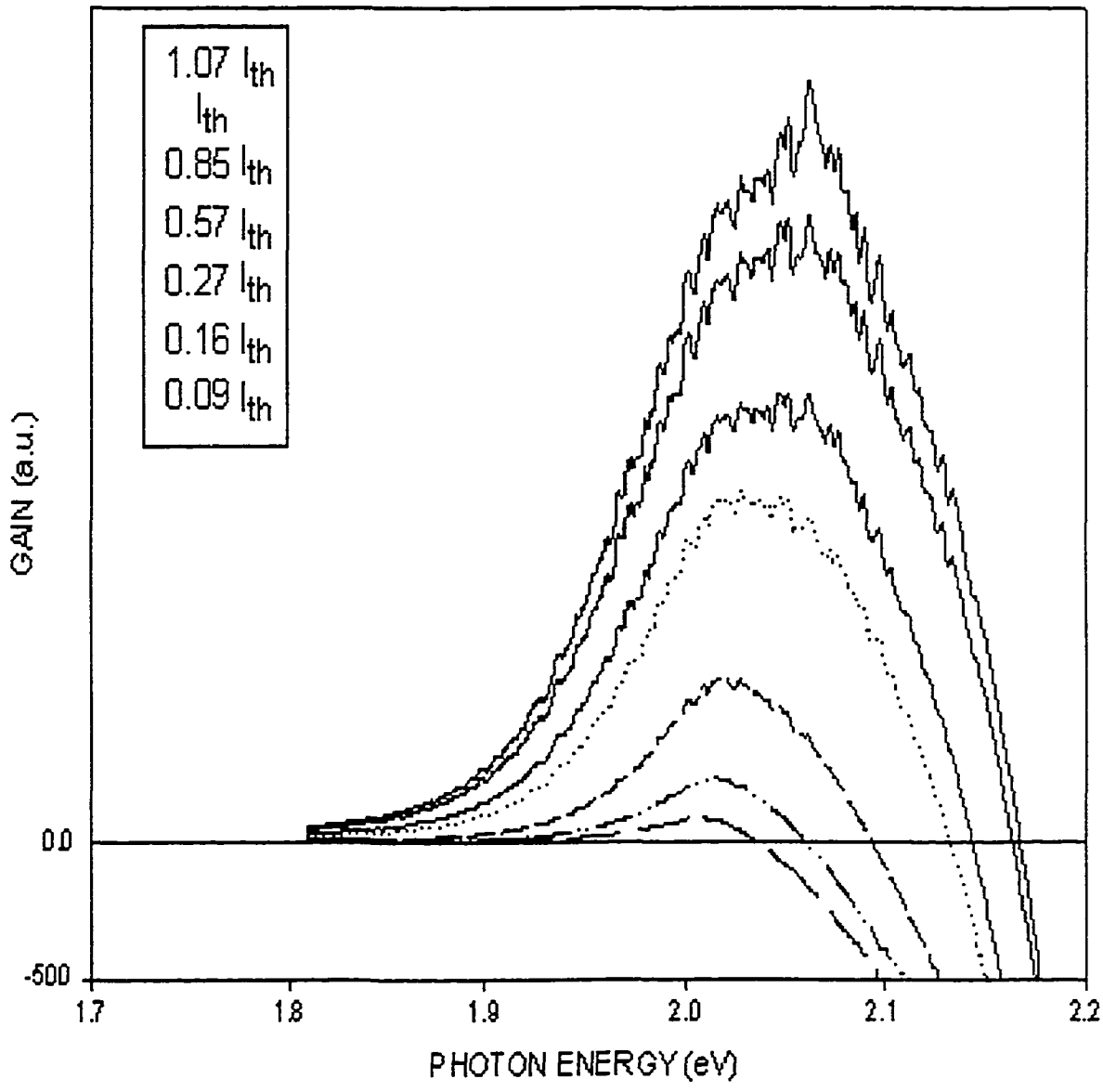

Figure 5.6 The gain profile constructed from the spontaneous emission spectra shown in Figure 5.3 at various pump intensities.

Chapter 6 Summary

This study was impelled by the wide interest in developingshort wavelength semiconductor light-emitting device for potential applications in data storage, display and laser printing. II-VI compound semiconductor materials have suitable bandgap energy to generate emission in the visible spectrum range. Most of the studies on II-VI compound light-emitting devices in recent years have been focused on the ZnCdSe/ZnSSe/ZnMgSSe material system grown on GaAs substrate. While having some success in MBE growth technique, p-doping technique and making metal-semiconductor contact, the overall device lifetime was still too short for practical applications. This study explored the possibilities of developing light emitting devices based on ZnCdSe/ZnCdMgSe material system grown on InP substrate. The major advantage of this material system is that all layers can be grown lattice-matched to the substrate to cover almost the entire visible spectrum.

In this thesis, I have presented the results of the photopumping experiment for ZnCdSe/ZnCdMgSe separate confinement semiconductor lasers structure grown on InP substrate. Photopumped laser operation has been realized in red, green and blue spectra range with ZnCdSe/ZndMgSe quantum-well

structures of different well thickness and/or composition. The full width at half maximum of laser peaks has typically a value less than 5 nm. The far-field intensity profile of the laser demonstrates the Gaussian pattern. The characteristic temperature, T_0, of the laser is about 150 K. This suggests that the potential barriers for the quantum well is sufficiently large to confine the carriers.

Light-emitting diodes (LED) fabricated from the same material systems have been investigated. The I-V measurement of the LED displays typical current-voltage characteristic for a diode with the turn-on voltage at about 4.5 V. The diode series resistance is on the order of 10 Ohms. The resistivity–thickness product (ρL) of the device is 2.5×10^{-2} Ohm•cm^2, where the resistivity is believed to be caused mainly by the p-side layers. In comparison, the corresponding ρL value for the state-of-the art GaAs laser is 4.2×10^{-4} Ohm•cm^2, which is two orders of magnitude smaller. Thus improving the conductivity of the p-layer and the quality of the p–contact remain a major challenge.

The electro-luminescence spectra taken from the surface of the LEDs show that in addition to the quantum-well emission at the predicted wavelength, there is a broad emission band centered at about 670 nm, which can be

attributed to the ZnSeTe p-contact layer. By removing most of the ZnSeTe layer, the red emission was greatly reduced or completely eliminated and the quantum well emission enhanced. The LEDs of various emission wavelength ranging from 520 nm to 610 nm have been demonstrated.

From the photoluminescence spectra, we constructed the optical gain spectra of the material using the method proposed by Henry et al. The spontaneous emission spectra show exponential decay when the photon energy is sufficiently higher than the absorption edge. The linear portion at high photon energy region of the spectra plotted in log scale was used to calculate the quasi-Fermi level separation. The width of gain profile is about 0.15 eV.

The results of the optical and electronic characterization presented in this thesis are qualitative because most of the parameters, such as effective masses and band offsets, of ZnCdMgSe material system are still unknown. This leaves a vast area for further studies. Improving the p-type doping to the quaternary ZnCdMgSe and making good Ohmic contact to reduce the resistivity are critical in fabricating diode lasers. With optimized structure design and improved conductivity in p-side layers, an electric pumped laser diode is expected to be realized in the near future.

References

[1] R.M. Park, M.B. Troffer, C.M. Rouleau, J.M. DePuydt, M.A. Hasse, "P-type ZnSe by nitrogen atom beam doping during molecular beam epitaxial growth", Appl. Phys. Lett. **57** (1990) 2127.

[2] K. Ohkawa, T. Karasawa, and T. Mitsuyu, "Characteritics of p-type ZnSe layers by molecular beam epitaxy with radical doping", Jpn. J. Appl. Phys., **30** (1991) L152-155.

[3] T. Yao, "Characterization of ZnSe grown by molecular beam epitaxy", J. Cryst. Growth, **72** (1985) 31-40.

[4] K. Ohkawa, T. Mitsuyu and O. Yamazaki, "Characteristics of Cl-doped ZnSe layers grown by molecular beam epitaxy", J. Appl. Phys., **62** (1987) 3216-3221.

[5] M.C. Tamargo, J.L. DeMiguel, D.M. Hwang and H.H. Farrell, "Structural characterization of GaAs/ZnSe interfaces", J. Vac. Sci. Technol., **B6** (1988) 784-787.

[6] H. Cheng, J.M. DePuydt, J.E. Potts and M.A. Haase, "Growth of p- and n-type ZnSe by molecular beam epitaxy", J. Cryst. Growth, **95** (1989) 512-516.

[7] J. Ren K.A. Bowers, B. Sneed, D.L. Dreifus, J.W. Cook Jr., J.F. Schetzina and R.M. Kolbas, "ZnSe light emitting diodes", Appl. Phys. Lett., **57** (1990) 1901-1903.

[8] M.A. Hasse, J. Qiu. J.M. DePuydt, H. Cheng, "Blue-green laser diodes", Appl. Phys. Lett. **59** (1991) 1272-1274.

[9] H. Okuyama, K. Nakano, T. Miyajima, Y. Morinaga, F. Hiei, M. Ozawa and K. Akimoto, "ZnSe/ZeMgSSe blue laser diode", Electron. Lett., **28** (1992) 1798.

[10] N. Nakayama, S. Itoh, S. Obata, K. Nakano, H. Okuyama, M. Ozawa, A. Ishibashi, M. Ikeda and Y. Mori, "Room temperature continuous operation of blue-green laser diode", Electron. Lett., **29** (1993) 1488-1489.

[11] J.M. Gaines, R.R. Drenten, K.W. Haberern, T. Marshall, P. Mensz and J. Petruzzello, "Blue-green injection lasers containing psedomorphic ZnMgSSe cladding layers and operating up to 394 K", Appl. Phys. Lett., **62** (1993) 2462-2464.

[12] H. Okuyama and A. Ishibashi, "Growth of ZnMgSSe and a blue laser diode", Microelectron. J., **25** (1994) 6443-649.

[13] S. Taniguchi, T. Hino, S. Itoh, K. Nakano, N. Nakayama, A. Ishibashi and M. Ikeda, "100h II-VI blue-green laser diode", Electron. Lett., **32** (1996) 552-553.

[14] S.Guha, H. Cheng, M. A. Hasse, J. M. Depuydt, J. Qiu, B. J. Wu, G. E. Hofler, "<100> dark line defect in II-VI blue-green light emitters", Appl. Phys. Lett. **65** (1994) 801-803.

[15] G. M. Haugen, S. Guha, H. Cheng, J. M. Depuydt, M. A. Hasse, G. E. Hofler, J. Qiu, and B. J. Wu, "Photodegradation of $Cd_xZn_{1-x}Se$ quantum-wells", Appl. Phys. Lett.. **66** (1995) 358-360.

[16] M. C. Tamargo, N. Dai, Cavus, R. Dzakpasu, W. Krystek, F. H.Pollak, F. Semendy, N. Bambha, P. Boyd, D. M. Hwang, and C.Y. Chen, SPIE Vol. **2346** (1994) 70.

[17] M. C. Tamargo, A. Cavus, L. Zeng , N. Dai, N. Bambha, A. Gray, F. Semedy, W. Krystek and F. H. Pollak, J. Electronic Materials **25** (1996) 259.

[18] T. Morita, A. Kikuchi, I. Nomura and K. Kishino, J. Electronic Materials **25** (1996) 425.

[19] A. Cavus, L. Zeng, M. C. Tamargo, N. Bambha, F. Semendy and A.Gray, Appl. Phys. Lett. **68** (1996).

[20] G.P. Agrawal and N.K. Dutta, "Long-wavelength semiconductor lasers", 72, Chapter 3.2, published by Van Nostrand Reinhold, New York, 1986.

[21] G.P. Agrawal and N.K. Dutta, "Long-wavelength semiconductor lasers", 37, Chapter 2.5, published by Van Nostrand Reinhold, New York, 1986.

[22] K. Ohkawa, T. Mitsuyu and O. Yamazaki, "Characteristics of Cl-doped ZnSe layers grown by molecular beam epitaxy", J. Appl. Phys. **62** (1987) 3216-3221.

[23] K.Ohkawa, T.karasawa and T.Mitsuyu, "Doping of nitrogen acceptors into ZnSe using a radical beam during MBE growth", J. Cryst. Growth, **111** (1991) 797-801.

[24] R.M. Park, M.B. Troffer, E. Yablonovitch, and T.J. Gmitter, "Non-contact electrical characterization of low-resistivity p-typeZnSe:N grown by molecular beam epitaxy", Appl. Phys. Lett., **59** (1991) 1896-1898.

[25] H. Jeon, J. Ding, W. Patterson A.V.Nurmikko, W. Xie, D.C. Grillo, M. Kobayashi and R.L. Gunshor, "Blue-green injection laser diodes in (Zn,Cd)Se/ZnSe quantum-wells", Appl. Phys. Lett., **59** (1991) 3619-3621.

[26] M. Kobayashi, R.L. Gunshor, A.V. Nurmikko and N. Otsuka, "The MBE growth of widegap II-VI injection lasers and LEDs", Optoelectronics, **7** (1992) 1-9.

[27] K. Okhawa, A. Tsujimura, S. Hayashi, S. Yoshii and T. Mitsuyu, "ZnSe-based laser diodes and p-type doping of ZnSe", Phys. B,**185** (1993) 112-117.

[28] S.Y. Wang, J. Simpson, H. Stewart, S.J.A. Adams, I. Hauksson, Y. Kawakami, M.R. Taghizadeh, K.A. Prior and B.C. Cavenett, "Photovoltage and carrier concentration profiles of ZnSe/ZnCdSe quantum-well laser diodes", Phys. B, **185** (1993) 508-511.

[29] Z. Yu, J. Ren, Y. Lansari, B. Sneed, K.A. Bowers, C. Boney, D.B. Eason, R.P. Vaudo, K.J. Gossett, J.W. Cook Jr. And J.F. Schetzina, "Light emission from quantum-well structures containing ZnS, ZnSe and related alloys", Jpn. J. Appl. Phys., **32** (1993) 663-668.

[30] J.M. Gaines, R.R. Drenten, K.W. Haberern, T. Marshall, P. Mensz and J. Petruzzelo, Appl. Phys. Lett., **62** (1993) 2462-2464.

[31] B.J. Fitzzpatrick, US patent 5 260 958 (1993).

[32] H. Okuyama, K, Nakano, T. Miyajima and K. Akimoto, "Epitaxial growth of ZnMgSSe on GaAs substrate by molecular beam epitaxy", Jpn. J. Appl. Phys., **30** (1991) L1620.

[33] K. Okuyama, F. Hiei and K. Akimoto, "Optically pumped blue lasing in ZnSe-ZnMgSSe double heterostructures at room temperature", Jpn. J. Appl. Phys., **31** (1992) L340-342.

[34] H. Okuyama, Y. Kishita, T. Miyajima, A. Ishibashi and K. Akimoto, "Epitaxial growth of p-type ZnMgSSe", Appl. Phys. Lett., **64** (1994) 904.

[35] H. Okuyama and A. Ishibashi, "Growth of ZnMgSSe and a blue-laser diode", Microelectron. J., **25** (1994) 643-649.

[36] H. Okuyama, K, Nakano, T. Miyajima and K. Akimoto, J. Crys. Growth, **117**(1992) 139.

[37] M.Ukita, H. Okuyama, M. Ozawa, A. Ishibashi, K. Akimoto and Y. Mori, Appl. Phys. Lett., **63** (1993) 2082.

[38] J.M. Woodall, J.L. Freeouf, G.D. Pettit, T. Jackson and P. Kirchner, J. Vac. Sci. Technol., **19** (1981) 626.

[39] Y. Fan, J. Han, L. He, J. Saraie, R.L. Gunshor, M. Hagerott, H. Jeon, A.V. Nurmikko, G.C. Hua and N. Otsuka, "A graded bandgap ohmic contact to p-ZnSe", Appl. Phys. Lett., **61** (1992) 3160-3162.

[40] A. Salokatve, H. Jeon, J. Ding, M. Hovinen, A.V. Nurmikko, D.C. Grillo, L. He, J. Han, Y. Fan, M. Ringle, R.L. Gunshor, G.C. Hua and N. Otsuka, Electron. Lett., **29** (1993) 2192.

[41] F. Hiei, M. Ikeda, M. Ozawa, T. Miyajima, A. Ishibashi and K. Akimoto, "Ohmic contacts to p-ZnSe using ZnTe/ZnSe multiquantum wells", Electron. Lett., **29** (1993) 878-879.

[42] M. Ozawa, F. Hiei, A. Ishibashi and K. Akimoto, Electron. Lett., **29** (1993) 503.

[43] S. Itoh, N. Nakayama, S. Matsumoto, M. Nagai, K. Nakano, M. Ozawa, H. Okuyama, S. Tomiya, T. Ohata, M. Ikeda, A. Ishibashi and Y. Mori, Jpn. J. Appl. Phys., **33** (1994) L938.

[44] T. Marshall, J. Gaines, J. Petruzzello, R. Drenten, P. Mensz and K. Haberren, in 7th IEEE Lasers and Electro-Opt. Society Annu. Meet., VS4.1, Boston, 1994.

[45] S. Kijima, H. Okuyama, Y. Sanaka, T. Kobayashi, S. Tomiya, and A. Ishibashi, "Optimized ZnSe:N/ZnTe:N contact structure of ZnSe-based II-VI laser diodes", Appl. Phys. Lett. **73** (1998) 235-237.

[46] E. Kato, H. Noguchi, M. Nagai, H. Okuyama, S. Kijima, and A.Ishibashi, Electron. Lett. **34** (1998) 282.

[47] G. M. Haugen, S. Guha, H. Cheng, J. M. DePuydt, M. A. Haase, G. E. Höfler, J. Qiu, and B. J. Wu, "Photodegradation of $Cd_xZn_{1-x}Se$ quantum wells", Appl. Phys. Lett., **66** (1995) 358-360.

[48] S. Guha, J. M. DePuydt, M. A. Haase, J. Qiu, and H. Cheng, "Degradation of II-VI based blue-green light emitters", Appl. Phys. Lett., **63** (1993) 3107-3109.

[49] S. Guha, H. Cheng, M. A. Haase, J. M. DePuydt, J. Qiu, B. J. Wu, and G. E. Hofler , "100 dark line defect in II-VI blue-green light emitters", Appl. Phys. Lett., **65** (1994) 801-803.

[50] G. C. Hua, N. Otsuka, D. C. Grillo, Y. Fan, J. Han, M. D. Ringle, and R. L. Gunshor, Appl. Phys. Lett. **65** (1994) 1331.

[51] M. Hovinen, J. Ding, A. Salokatve, A. V. Nurmikko, G. C. Hua, D. C. Grillo, L. He, J. Han, M. Ringle, and R. L. Gunshor, J. Appl. Phys. **77** (1995) 4150.

[52] S. Guha, J. M. DePuydt, J. Qiu, G. E. Hofler, M. A. Haase, B. J. Wu, and H. Cheng , "Role of stacking faults as misfit dislocation sources and nonradiative recombination centers in II-VI heterostructures and devices", Appl. Phys. Lett., **63** (1993) 3023-3025.

[53] M. Hovinen, J. Ding, A. V. Nurmikko, G. C. Hua, D. C. Grillo, L. He, J. Han, and R. L. Gunshor, Appl. Phys. Lett. **66** (1995) 2013.

[54] K. Nakano, S. Tomiya, M. Ukita, H. Yoshida, S. Itoh, E. Morita, M. Ikeda, and A. Ishibashi, J. Electron. Mater. **25** (1995) 21.

[55] L. H. Kuo, L. Salamanca-Riba, B. J. Wu, G. M. Haugen, J. M. DePuydt, G. Hofler, and H. Cheng, J. Vac. Sci. Technol. B, 13, 1694 (1995).

[56] J. Petruzzello, K. Haberern, S. Herko, T. Marshall, S. Guha, G. U'Ren, and G. M. Haugen, J. Cryst. Growth **159** (1996) 573.

[57] L.-L. Chao, G. S. Cargill III, C. Kothandaraman, T. Marshall, E. Snoeks, M. Buijs, K. Haberern, J. Petruzzello, G. M. Haugen and K. K. Law, "Activation energy of nonradiative processes in degraded II-VI laser diodes", Appl. Phys. Lett., **70** (1997) 535-537.

[58] L. H. Kuo, L. Salamanca-Riba, B. J. Wu, G. Hofler, J. M. DePuydt, and H. Cheng, Appl. Phys. Lett., **67** (1995) 3298.

[59] C.C. Chu, T.B. Ng, J. Han, G.C. Hua, R.L. Gunshor, E. Ho, E. L. Warlick, L.A. Kolodziejski and A.V. Nurmikko, "Reduction of structural defects in II-VI blue green laser diodes", Appl. Phys. Lett., **69** (1996) 602.

[60] F.S. Turco-Sandroff, R.E. Nahory, M.J.S.P. Brazil, R.J. Martin, R. Beserman, L.A. Farrow, J.M. Worlock and A.L. Weaver, J. Cryt. Growth, 111 (1991) 762.

[61] M.C. Tamargo, R. Hull, L.H. Greene, J.R. Hayes and A. Y. Cho, Appl. Phys. Lett., **46** (1985) 569.

[62] L.L. Chao, H. Xing, G.S. Cargill III, L. Zeng and M.C. Tamargo, Bullitin of the American Physical Society, **43** (1998) 718. APS March Meeting, Los Angeles, CA., USA.

[63] M. Lomascolo, G.H. Li, K. Syassen, R. Cingolani, and I. Suemune, "Pressure-induced conduction-band crossover in a $ZnSe/ZnS_{0.18}Se_{0.82}$ symmetric superlattice", Phys. Rev. B., **50** (1994) 14635-14638.

[64] K. Shahzad, H, Petruzzello, J.M. Gaines, and C. Ponzoni, "An investigation of energy-band offsets in the $ZnSe/Zn_{1-x}Mg_xS_ySe_{1-y}$ multiquantum-wells system", Appl. Phys. Lett., **67** (1995) 659-661.

[65] R. Cingolani, P. Prete, M. Lomascolo, G. Coli, L. Calcagnile, N. Lovergine, G. Salviati, and L. Lazzarini, "Impact of electron confinement on the lasing properties of ZnS/ZnSe superlattices", Appl. Phys. Lett., **70** (1997) 2943-2945

[66] T. Miyajima, F.P. Logue, J.F. Donegan, J. Hegarty, H. Okuyama, A. Ishibashi, and Y. Mori, "Quasi-two-dimensional exciton in ZnSe/ZnMgSSe single quantum-well", Appl. Phys. Lett., **66** (1995) 180-182.

[67] W. Ossau, B. Kuhn-Heinrich, A. Waag, T. Litz, G. Landwchr, "Valence band offset in semimagnetic CdTe/(CdMn)Te quantum-wells", Superlattices and Microstructures, **15** (1994) 503-507.

[68] A. Ishibashi, "II-VI blue-green laser diodes", IEEE J. Selected topics in Quantum Electron., **1**, (1995) 741-748.

[69] H. Kressel and M. Ettenberg, Appl. Phys. Lett.,**23** (1973) 511.

[70] N. Dai, A. Cavus, R. Dzakpasu, M.C. Tamargo, F. Semendy, N. Bambha, D.M. Huang and C.Y. Chen, "Molecular beam epitaxial growth of high quality $Zn_{1-x}Cd_xSe$ on InP substrates", Appl. Phys. Lett., **66** (1995) 2742-2744.

[71] Y. Guo, G. Aizin, Y.c. Chen, L. Zeng, A. Cavus, and M.C. Tamargo, "Photo-pumped ZnCdSe/ZnCdMgSe blue-green quantum well lasers grown on InP substrates", Appl. Phys. Lett., **70** (1997) 1351-1353.

[72] M. Ukita, H. Okuyama, M. Ozawa, A. Ishibashi, K. Akimoto, and Y. Mori, Appl. Phys. Lett. **63** (1993) 2082.

[73] H. Okuyama, F. Hiei, K. Akimoto, Jpn. J. Appl. Phys. **31** (1992) L340.

[74] T. R. Chen, B. Chang, L. C. Chiu, K. L. Yu, S. Margalit and A. Yariv, Appl. Phys. Lett., **43** (1983) 217.

[75] L. C. Chiu, K. L. Yu, S. Margalit, T. R. Chen, U. Koren, A. Hasson and A. Yariv, IEEE J. Quantum Electron. **QE-19** (1983) 1335.

[76] G. H. B. Thompson, IEE Proc., I **128** (1981) 37.

[77] A. Sugimura, IEEE J. Quantum Electron., **QE-17** (1981) 441.

[78] L.Zeng, B.X.Yang, A. Cavus, W. Lin, Y.Y. Luo, M.C. Tamargo, Y. Guo, and Y.C. Chen, "Red-green-blue photopumped lasing from ZnCdMgSe/ZnCdSe quantum well laser structures grown on InP", Appl. Phys. Lett., 72 (1998) 3135-3138.

[79] M. C. Tamargo, A. Cavus, L. Zeng, B. Yang, F. Semendy, A. Gray, N. Bambha, E. Snoeks and L. Zhao, presented at the 1996 Spring Materials Research Society Meeting, San Francisco, CA, April 10, 1996.

[80] W.Faschinger, S. Ferreira and H. Sitter, "Doping of zinc-selenium-telluride", Appl. Phys. Lett., **64** (1994) 2682-2684.

[81] S. Wei and A. Zunger, Appl. Phys. Lett., **72** (1998) 2011.

[82] H. Luo and J. K. Furdyna, Semicond. Sci. Technol., **10** (1995) 1041.

[83] H. Iwata, K. Naniwae and K. Yashiki, "MgZnSeTe/ZnCdSe/MgZnCdSe double heterostructure light-emitting diodes", Proceeding of SPIE , **3285** (1998) 5.

[84] D. Lee, A. Mysyrowicz, A. V. Nurmikko and B. J. Fitzpatrick, "Exciton self-trapping in ZnSe-ZnTe alloys", Phys. Rev. Lett., **14** (1987) 2127.

[85] C. H. Henry, R. A. Logan, and F. R. Merritt, "Measurement of gain and absorption spectra in AlGaAs buried heterostructure lasers", J. Appl. Phys. **51** (1980) 3042-3050.